



Review Article

Quantifying rates of landscape evolution and tectonic processes by thermochronology and numerical modeling of crustal heat transport using PECUBE

Jean Braun ^{a,*}, Peter van der Beek ^a, Pierre Valla ^{a,c}, Xavier Robert ^a, Frédéric Herman ^c, Christoph Glotzbach ^d, Vivi Pedersen ^e, Claire Perry ^b, Thibaud Simon-Labré ^{a,f}, Cécile Prigent ^g

^a Institut des Sciences de la Terre, Université Joseph Fourier, CNRS, Grenoble, France

^b GEOTOP, Université du Québec à Montréal, Canada

^c Geologisches Institut, Eidgenössische Technische Hochschule (ETH), Zürich, Switzerland

^d Institute of Geology, Leibniz University, Hannover, Germany

^e Department of Earth Sciences, Aarhus University, Denmark

^f Institut de Géologie et Paléontologie, Université de Lausanne, Switzerland

^g Laboratoire des Sciences de la Terre, Ecole Normale Supérieure, Lyon, France

ARTICLE INFO

Article history:

Received 15 March 2011

Received in revised form 14 November 2011

Accepted 21 December 2011

Available online 29 December 2011

Keywords:

Quantitative thermochronology

PECUBE

Numerical modeling

Heat transfer in the crust

Low-temperature thermochronology

ABSTRACT

PECUBE is a three-dimensional thermal-kinematic code capable of solving the heat production-diffusion-advection equation under a temporally varying surface boundary condition. It was initially developed to assess the effects of time-varying surface topography (relief) on low-temperature thermochronological datasets. Thermochronometric ages are predicted by tracking the time-temperature histories of rock-particles ending up at the surface and by combining these with various age-prediction models. In the decade since its inception, the PECUBE code has been under continuous development as its use became wider and addressed different tectonic-geomorphic problems. This paper describes several major recent improvements in the code, including its integration with an inverse-modeling package based on the Neighborhood Algorithm, the incorporation of fault-controlled kinematics, several different ways to address topographic and drainage change through time, the ability to predict subsurface (tunnel or borehole) data, prediction of detrital thermochronology data and a method to compare these with observations, and the coupling with landscape-evolution (or surface-process) models. Each new development is described together with one or several applications, so that the reader and potential user can clearly assess and make use of the capabilities of PECUBE. We end with describing some developments that are currently underway or should take place in the foreseeable future.

© 2012 Elsevier B.V. All rights reserved.

Contents

1. Introduction	2
2. Initial version of PECUBE	3
3. Basic developments	4
3.1. Partial differential equation	4
3.2. Age prediction models	4
3.3. Isostasy	4
3.4. Bilinear uplift function	5
4. Inversion	5
4.1. Inversion Example 1: A synthetic problem	7
4.1.1. Problem setup	7
4.1.2. Results	8

* Corresponding author. Tel.: +33 0 476 51 40 74; fax: +33 0 476 51 40 58.

E-mail addresses: Jean.Braun@ujf-grenoble.fr (J. Braun), pvdbeek@ujf-grenoble.fr (P. van der Beek), Pierre.Valla@ujf-grenoble.fr (P. Valla), Xavier.Robert01@gmail.com (X. Robert), frederic@erdw.ethz.ch (F. Herman), glotzbach@geowi.uni-hannover.de (C. Glotzbach), vivi.pedersen@geo.au.dk (V. Pedersen), Claire@uqam.ca (C. Perry), Thibaud.Simon-Labré@unil.ch (T. Simon-Labré), Cécile.Prigent@ens-lyon.fr (C. Prigent).

4.2.	Inversion Example 2: Constraining relief evolution in a tectonically active area, the Southern Alps of New Zealand	8
4.2.1.	Motivation	8
4.2.2.	A very low temperature system	9
4.2.3.	OSL dataset to constrain recent relief change	10
5.	Borehole/tunnel data	11
5.1.	Motivation	11
5.2.	Implementation in PECUBE	12
5.3.	Synthetic dataset	12
5.4.	Example: Mont Blanc tunnel transect	13
6.	Faulting	15
6.1.	Motivation	15
6.2.	Definition of faults in PECUBE	15
6.2.1.	Reference frame	15
6.2.2.	Fault geometry	15
6.2.3.	Fault kinematics	16
6.2.4.	Multiple faults	17
6.3.	Faulting example: Faulting sequence in central Nepal	17
6.3.1.	Model setup	17
6.3.2.	Effect of out-of-sequence thrusting on thermochronological age patterns	18
7.	Detrital thermochronology	19
7.1.	Motivation	19
7.2.	Generation of predicted detrital age distributions	19
7.3.	Comparing PECUBE predictions to observed detrital distributions	20
7.4.	Case study: Analyzing the detrital thermochronology record in the Siwaliks of Nepal	20
8.	Linking PECUBE to a landscape-evolution model	21
8.1.	Motivation	21
8.2.	Working procedure	21
8.3.	Example: Combining PECUBE with a fluvio-glacial SPM	22
9.	Future improvements	22
9.1.	More detailed thermal structure	22
9.2.	Complex velocity fields	25
9.3.	Better coupling with surface-process models	25
9.4.	Advanced age-prediction models	25
10.	Conclusion and code availability	26
	Appendix A. Supplementary data	26
	References	26

1. Introduction

In recent years, major advances have been made in the development of low temperature thermochronological techniques (e.g., Flowers et al., 2009; Gautheron et al., 2009; Herman et al., 2010b; Ketcham et al., 2007; Shuster and Farley, 2004). These advances allow us to answer in more detail questions pertaining to the processes by which rocks are cooled on their way to the surface, i.e. tectonic exhumation and/or surface erosion. These are, in turn, linked to the processes by which surface landforms evolve through time (Braun, 2002b; Brown et al., 1994; Ehlers and Farley, 2003; Gunnell, 2000). Such questions include: what is the rate of river incision or knickpoint retreat along a channel profile? What is the age of a landform? How efficient is glacial erosion compared to river incision? How rapidly does a landscape respond to a change in tectonic uplift/convergence or a climate change? What controls spatial and temporal variations in tectonic/surface processes? Many others can be, and have been, posed.

Although it may seem obvious to use the information derived from low-temperature thermochronology to constrain the rate at which rocks move to the surface or, conversely, the rate at which the surface topography evolves through time, this approach has led to a major challenge: can we describe or predict with sufficient accuracy the temperature structure in the Earth's upper crust to infer exhumation rate from cooling rate? This challenge is augmented when one realizes that the process of exhumation itself perturbs the temperature structure, as does the finite amplitude topography that we wish to measure or date. Other challenges, inherent to any modeling exercise that attempts to reproduce data, include the knowledge we have of the physical processes at play in setting the thermochronological

age during cooling of the rock sample, as well as the uncertainty associated with noise in the data.

Consequently, the development of quantitative interpretation methods has paralleled the evolution of thermochronological techniques (Adams, 1981; Batt and Brandon, 2002; Batt and Braun, 1997; Bollinger et al., 2006; Braun, 2002a, 2003; Ehlers et al., 2003; Stüwe et al., 1994). The effect of rock advection and simple (periodic) finite-amplitude topography on the temperature structure of the crust is now commonly considered in the interpretation of thermochronological data (Herman et al., 2010b, for example). Sophisticated methods have been developed to interpret more accurately data from, for example, boreholes or tunnels (Foeken et al., 2007; Gallagher et al., 2005; Glotzbach et al., 2011), age-elevation profiles (Bermúdez et al., 2011; Valla et al., 2010), gradients in ages across faults (Campani et al., 2010; Ehlers et al., 2001; Robert et al., 2009), or detrital age datasets (Avdeev et al., 2011; Brewer et al., 2003; Rahl et al., 2007; Vermeesch, 2007; Whipp et al., 2009).

The authors of this paper have contributed to such methods through the development of a numerical model, PECUBE (Braun, 2003), initially designed to predict the 3D thermal structure of the crust in regions subject to complex exhumation and landform-evolution histories (Fig. 1). In the past 5 yr, this numerical model has evolved and we have felt the need to update the low-temperature thermochronology community of its current abilities (and limitations). This is the main purpose of this paper, but we also wish to give the reader an overview of what can be achieved with PECUBE through the description of a few of the studies we have accomplished in recent years.

The paper is organized in sections, each describing a novel aspect in the methodological development of interpretation techniques. In

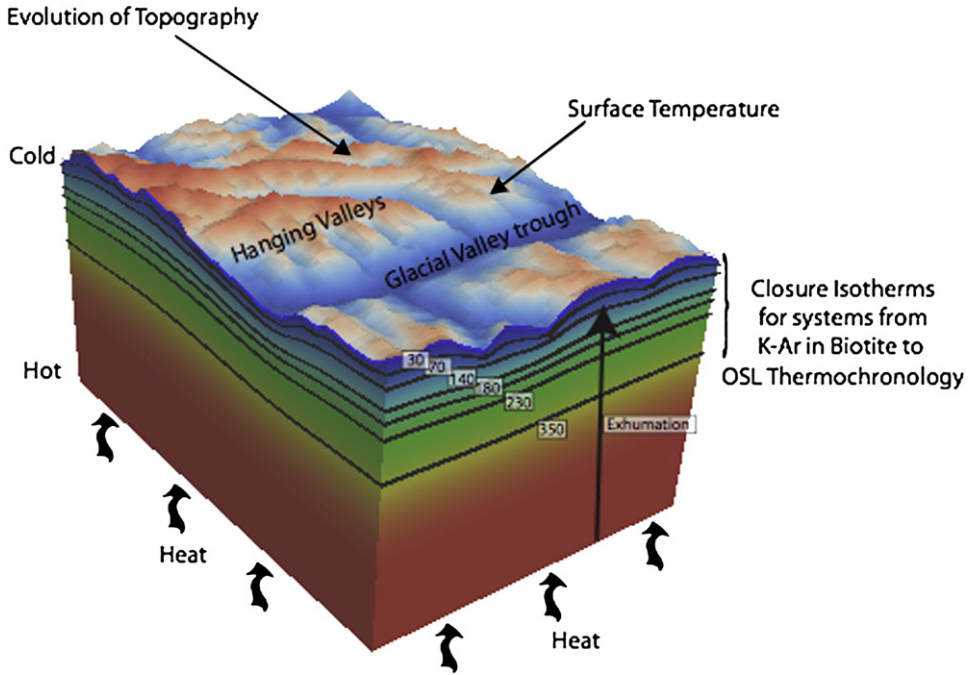


Fig. 1. Basic philosophy of the PECUBE model. Shown is a crustal block, subjected to a uniform uplift rate and assuming a time-varying, finite amplitude surface topography. The sides of the block show the thermal structure (note the compression of isotherms near the surface as a result of rapid rock advection). In black are shown the isotherms corresponding to various thermochronometers. Ages can be predicted for each thermochronometer, from temperature histories obtained by following rock particle paths (vertical black arrow) and interpolating the temperature field onto the rock position. Predicted ages can be compared to data collected in the region.

each section, we provide a short account of the circumstances in which the development was made, i.e. the new question that we were trying to address or the interpretation problem or dilemma that we were facing, we explain the method and, if necessary, its underlying numerical implementation, and we provide one or several examples of its application by using real datasets, which were in many cases purposely collected. Most of these datasets and their interpretations are published. Included with the paper as supplementary material are the user guide and a set of input files and data files that are based on relatively simpler applications and that can serve to familiarize a new user with PECUBE.

2. Initial version of PECUBE

In its original version (Braun, 2003), PECUBE was designed to solve the three-dimensional heat-transfer equation in a crustal block, but in which the advection term is limited to be vertical:

$$\frac{\partial T}{\partial t} + \dot{E} \frac{\partial T}{\partial z} = \frac{\partial}{\partial x} \kappa \frac{\partial T}{\partial x} + \frac{\partial}{\partial y} \kappa \frac{\partial T}{\partial y} + \frac{\partial}{\partial z} \kappa \frac{\partial T}{\partial z} + A. \quad (1)$$

Heat production A was assumed constant and uniform; κ is thermal diffusivity. PECUBE explicitly decouples rock uplift from surface evolution (see below) so that \dot{E} is rock-uplift rate (in the sense of England and Molnar (1990)) with respect to the base of the model. The local exhumation rate will be the difference between this regional rock-uplift rate and changes in local surface elevation resulting from the imposed relief-evolution scenario. In case of steady-state topography (no relief changes), \dot{E} becomes the exhumation rate. The initial temperature condition is the steady-state solution computed from the imposed initial geometry and velocity field. In the remainder of this paper (as in most of our previous publications) we will refer to \dot{E} as the “mean” or “regional” exhumation rate.

The main advance proposed by PECUBE, and the motivation behind its development, were its ability to accurately predict the thermal perturbation caused by a finite-amplitude, time-varying

surface topography. Simple point advection methods were used to track the path of rock particles that were exhumed at the surface of the model at the end of the model run. Using the thermal histories obtained by interpolating the temperature field onto rock particle positions at the end of each time step, the user could predict cooling ages for any thermochronological system.

In this form, PECUBE was used to predict the distribution of ages that would result from a combination of regional rock-uplift rates and rates of relief change (Braun, 2002b). It provided the insight and quantitative confirmation that independent information can be extracted from the distribution of ages at the surface of the Earth about the mean rate of exhumation (rock-uplift rate under steady-state topography) and the rate of relief change, or the “age” of the landform (Braun, 2002b). These findings were accompanied by the development of a spectral method (Braun, 2002a) that demonstrated that the relationship between age and elevation must be considered as a function of the wavelength of the landforms on which it is collected. Short-wavelength age-elevation relationships inform us on the mean exhumation rate, independently of any change of the landform, whereas long-wavelength relationships contain information on the rate of change of relief, i.e. whether it grew or decreased in amplitude since the mean age of the thermochronological dataset.

PECUBE was also used to demonstrate that the sampling must be preferentially performed in a direction perpendicular to the main relief (i.e. across the dominant features of the landform – valleys and interfluves) and thus, most commonly, perpendicular to the direction of tectonic transport, which implies that the data must be interpreted using a three-dimensional representation of the temperature field (Braun, 2002a) that takes into account simple geographical variations in relief, relief evolution and tectonic uplift. Furthermore, in many instances, the topography that is being constrained (or more exactly its age) by using PECUBE is itself often complex and its three-dimensional effect on the underlying thermal structure must be taken into account. See, for example, the recent use of PECUBE to interpret the evolution of glacial landform in the South Island, New Zealand, by Shuster et al. (2011).

These methods were used to constrain the age of Kings Canyon in the Sierra Nevada (Braun, 2002a), the age of the high relief topography in the central part of the Southern Alps, New Zealand (Herman et al., 2007), and other locations and settings (Braun and Robert, 2005; Braun and van der Beek, 2004). Most of these results and advances have been described in a textbook (Braun et al., 2006).

In the years following its publication and release, PECUBE has been widely used by the thermochronological community and, consequently, has been updated and improved to respond to a variety of needs expressed by that community. These improvements were, in part, developed by the community of users and an effort was undertaken to assemble those changes into a new version that was released at the 12th International Conference on Thermochronology in Glasgow in August 2010. The following sections of this paper explain these improvements in detail and how they have been implemented in PECUBE. They also illustrate how these modifications improve the quality of the interpretation of thermochronological datasets through a series of case examples.

3. Basic developments

3.1. Partial differential equation

The basic heat transport equation solved in PECUBE was generalized to include all three advection terms:

$$\frac{\partial T}{\partial t} + u \frac{\partial T}{\partial x} + v \frac{\partial T}{\partial y} + w \frac{\partial T}{\partial z} = \frac{\partial}{\partial x} \kappa \frac{\partial T}{\partial x} + \frac{\partial}{\partial y} \kappa \frac{\partial T}{\partial y} + \frac{\partial}{\partial z} \kappa \frac{\partial T}{\partial z} + A \quad (2)$$

where u, v, w are the component of a general velocity field representing the relative motion of rock with respect to a fixed base. In cases where uniform vertical uplift only is specified, we have: $u = v = 0$ and $w = \dot{E}$, as in the initial PECUBE version. In cases where uplift varies spatially, w is a function of the horizontal coordinates x, y . In cases where rocks are advected by the relative motion of rock masses along one or several faults, u, v and w must be defined. We show how this has been implemented in Section 6.

This equation is solved by the finite element method, using 6- or 8-node prismatic elements (as described in Braun (2003)) that are linear in the vertical direction and linear or bilinear in the horizontal directions.

3.2. Age prediction models

The philosophy in PECUBE has always been to predict thermochronological ages from the time–temperature histories of rock particles (obtained from the solution of the heat-transport equation and the interpolation of the resulting temperature field) using forward kinetic models rather than a simple closure-temperature approach.

To obtain the temperature histories, we first run PECUBE backward in time, without calculating the temperature field but by advecting points that are first positioned on a regular grid at the surface of the model, using the velocity field (u, v, w) defined above in a simple, first-order accurate procedure. PECUBE is then run forward in time, i.e. the temperature field is calculated by solving Eq. (2) at a set of predefined time intervals, and the position of the points advected during the first phase of computation, is updated by using the same advection procedure in reverse. Note that because the velocity field is now fully three-dimensional, the points are located at arbitrary locations and a full three-dimensional interpolation procedure is needed to transfer the temperature from the nodes of the finite element mesh to these arbitrary locations. We use the fact that the elements are organized in vertical columns to perform this operation in an efficient manner, making use of an extension in three dimensions of the walking triangle algorithm (Lawson, 1977).

The initial version of PECUBE included modules to predict (U-Th)/He and fission-track ages in apatite, as well as mica Ar–Ar ages, using modeling approaches outlined in Braun et al. (2006). Over the years, a number of routines have been added to PECUBE to model a wide range of thermochronological systems and some of the kinetic models have changed. The current version of PECUBE includes the following age-prediction models:

- (U-Th-Sm)/He ages in apatite (AHe) and zircon (ZHe) are predicted using the numerical scheme of Wolf et al. (1998) and the kinetic parameters of Farley (2000) for apatite and Reiners et al. (2004) for zircon, respectively, assuming a 100 μm grain size;
- K-Ar (or Ar–Ar) ages in biotite, muscovite, hornblende and K-feldspar are predicted using the same numerical production-diffusion model as for (U-Th-Sm)/He and kinetic parameters from Grove and Harrison (1996) for biotite, Hames and Bowring (1994) for muscovite and Harrison (1981) for hornblende, respectively, assuming a 500 μm grain size. K-feldspar ages are predicted using the kinetic parameters of Lovera et al. (1991) for their MH-10 sample and assuming a single diffusion domain; multi-domain diffusion is not implemented as yet;
- Fission-track ages in apatite (AFT) and zircon (ZFT), and fission-track length distributions in apatite, are predicted using several different models and parameterizations. For apatite, either the “linear-fanning” model of Green et al. (1989), with kinetic parameters from Crowley et al. (1991); Laslett et al. (1987) or Stephenson et al. (2006), or the “fanning curvilinear” model and overall kinetic parameters of Ketcham et al. (1999) can be used. For the zircon fission-track system, the annealing model of Galbraith and Laslett (1997) is used, with annealing parameters from either Rahn et al. (2004) (zero-damage zircon) or Tagami et al. (1998) (α-damaged zircon).

The user can choose what ages to predict and what models to use to predict the age of a particular thermochronologic system, based on the characteristics of the particular dataset (s) he wishes to compare the PECUBE predictions to. The implementation of age-prediction models is constantly in progress (see Section 9). Note, however, that predictive models will never be perfect, a point which must be kept in mind when comparing model predictions with observations.

3.3. Isostasy

The post-orogenic relief evolution of many mountain belts remains enigmatic: in many instances, rugged relief survives the cessation of tectonic activity for many tens of millions of years. Examples include the Dabie Shan of eastern China (Braun and Robert, 2005) or the Sierra Nevada of Western North America (Braun, 2002a; House et al., 1998) where kilometer-scale topographic relief potentially survived for 60 to 80 Myr after the end of the orogenic phase. The key to understand such longevity of topography lies in part in the isostatic response to surface erosion. Assuming local isostatic equilibrium, one can easily show that, to reduce surface topography by one kilometer, up to 6 km of erosion is required (England and Molnar, 1990). This ratio between reduction of surface elevation, Δe and isostatic uplift u is set by the ratio of the density difference between crustal and mantle rocks, $\Delta\rho$ and mean density of crustal rock ρ_c :

$$\frac{\Delta e}{u} = \frac{\Delta\rho}{\rho_c}. \quad (3)$$

Note that this relationship assumes that the rate at which isostatic uplift takes place is similar to or smaller than the conductive cooling rate of the lithosphere such that lithospheric thickness can be assumed to remain constant.

The continental lithosphere is, however, characterized by a finite flexural strength such that its isostatic response to changes in surface

topography is spread over a finite distance of several tens to hundreds of kilometers (Forsyth, 1985). In order to provide quantitative estimates of the isostatically driven rock uplift associated with lowering of topography, we added a flexural isostasy module to PECUBE, which solves the following bi-harmonic equation:

$$D \frac{\partial^4 \Delta u}{\partial x^4} + D \frac{\partial^4 \Delta u}{\partial y^4} + 2D \frac{\partial^4 \Delta u}{\partial x^2 \partial y^2} = \Delta \rho g \Delta u + \rho_c g \Delta e \quad (4)$$

where D is the flexural rigidity given by:

$$D = \frac{ET_e^3}{12(1-\nu^2)}. \quad (5)$$

T_e is equivalent elastic thickness of the plate, E is Young's modulus, ν is Poisson's ratio, g is the acceleration due to gravity and Δe and Δu are the increment in surface topography and uplift over a time step Δt of computation. We use an efficient Fourier-transform approach to solve this so-called "thin elastic plate equation" (Nunn and Aires, 1988), which requires, however, that the flexural rigidity be uniform.

The solution Δu is then used to compute an additional component to the rock uplift rate given by $\Delta u/\Delta t$. The elastic plate thickness, T_e , as well as the elastic parameters (Young modulus and Poisson's ratio) can be tuned at will. Note that flexural isostasy occurs in response to changes in surface topography, not to mean exhumation. In the implementation chosen in PECUBE, rock uplift induced by isostasy is added to the rock uplift and thus leads to additional exhumation induced by temporal changes of the (independently imposed) surface. This addition to PECUBE has been successfully used to constrain the age of relief in the Dabie Shan and to demonstrate that quantitative constraints can be derived about the strength of the lithosphere from the spatial distribution of low temperature thermochronological data (Braun and Robert, 2005).

3.4. Bilinear uplift function

Some tectonic settings are better represented by smoothly varying uplift functions, for example to represent tilting rather than uniform uplift of a piece of continental crust. For this reason, we included the possibility to impose a set uplift rate (u) at the four corners of the rectangular region in which PECUBE solves the heat equation ($u_i, i=1,\dots,4$). These values are in turn interpolated by a simple bilinear function to other parts of the region:

$$u(r,s) = \sum_{i=1}^4 N_i(r,s) u_i \quad (6)$$

where:

$$\begin{aligned} N_1(r,s) &= (1-r)(1-s)/4 \\ N_2(r,s) &= (1+r)(1-s)/4 \\ N_3(r,s) &= (1+r)(1+s)/4 \\ N_4(r,s) &= (1-r)(1+s)/4 \end{aligned} \quad (7)$$

and the r,s -coordinates define a linear mapping between each of the x,y coordinates of the corners of the rectangular area over which PECUBE solves the heat equation and the interval $[-1, +1]$ (see Fig. 2). Such a function cannot be used, however, to represent discontinuities such as faults; these have been dealt with through the addition of a new faulting model in PECUBE (see Section 6).

4. Inversion

In general, a thermochronologist will use PECUBE because (s)he is interested in finding the exhumation and relief histories that are most compatible with his/her data. These histories can be represented by a

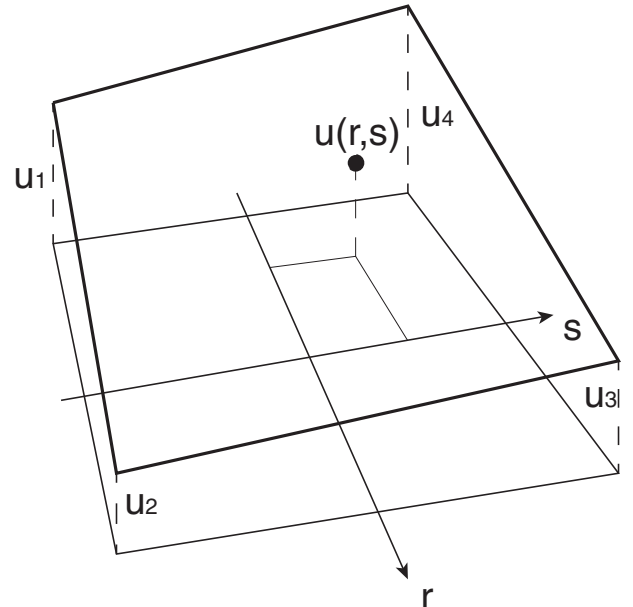


Fig. 2. The bilinear uplift function (thick line) defined from imposed uplift values defined at the four corners of the PECUBE domain, using the global (r,s) coordinates.

combination of model input parameters, typically a limited number of "phases" of exhumation, characterized by an onset and an end time, and an exhumation rate. However, given the potentially unlimited number of possible scenarios and the large number of parameter values that could potentially vary, one often needs to run a very large number of models in order to explore the parameter space, which rapidly becomes excessively time-consuming. A more efficient approach is inverse modeling (e.g. Tarantola, 2005), in which the general goal is to assess the resolution of (or information contained in) a thermochronological dataset to constrain exhumation and relief histories and/or other parameters such as geothermal gradient, flexural rigidity, etc.

Inverse modeling of thermochronological datasets is rapidly becoming more widely used (e.g. Braun and Robert, 2005; Braun and van der Beek, 2004; Herman et al., 2007; Gallagher et al., 2005; Campani et al., 2010; Herman et al., 2010a,b; Valla et al., 2010; van der Beek et al., 2010; Avdeev et al., 2011; Robert et al., 2011; Valla et al., 2011, 2012; Glotzbach et al., 2011). Here, we describe a recently developed approach combining PECUBE with the inverse method NA (Neighborhood Algorithm by Sambridge, 1999a, b). This method uses a two-step approach to:

1. extract optimal (i.e. best-fitting) denudation/relief scenarios and thermal/flexural parameters from thermochronology data (the "NA sampling stage");
2. derive estimates of the precision with which denudation rates, timing of rate changes, relief evolution, and/or thermal/flexural parameters are resolved (the "NA appraisal stage"), taking into account the sensitivity of the model (or parameterization) to the available age data as well as the error associated with each data point.

The latest PECUBE version includes full implementation of the NA code, allowing to use the same package in either forward or inverse mode. For the user, the inversion mode is automatically selected when any of the parameters appears as a range (two numbers separated by a colon) rather than a single value in one of the input files (see the User Guide in Appendix 1, Supplementary Online Material, for further details). Basics of inverse theory and other concepts behind the NA approach, as well as code specifics and statistical assumptions, are fully described by (Sambridge, 1999a, b). In the following, we will

briefly describe the 2-step NA approach and provide some details of the input parameters controlling the inversion procedure.

Generally, the inverse mode combining PECUBE with the NA approach consists in defining tectono-geomorphic scenarios (exhumation and/or relief evolution) and thermo-kinematic parameters to be explored within a-priori defined ranges. The sampling stage iteratively samples the prior model space to find the parameter combinations that yield the smallest misfit between observed and predicted data. In an initial step, the parameter space is randomly sampled and sub-divided into individual Voronoi cells with corresponding misfit values, yielding misfit surfaces. Subsequent sample iterations make use of these misfit surfaces by concentrating re-sampling in areas (Voronoi cells) with a better misfit rank. Three parameters control the sampling stage: (i) the number of iterations, (ii) the number of models generated at each iteration and (iii) the number of Voronoi cells resampled at each iteration. Note that model-parameter predictions are sensitive to these parameters as they control the way the inversion procedure will explore the multi-dimensional parameter space. There is no strict rule to choose these parameters but, in general, models with a higher complexity require more iterations. Depending on the inverse model complexity, our experience suggests that running ~10,000 PECUBE forward models (i.e. 100 iterations of 100 model runs each) may provide optimal convergence when used to invert for 5 to 6 model parameters. This number increases dramatically with the number of parameters inverted for. A high resampling ratio (i.e., ratio between the number of Voronoi cells resampled and the total number of models in each iteration) leads the sampling algorithm to be more explorative and less exploitative (Sambridge, 1999a). Decreasing the ratio between the number of Voronoi cells re-sampled and the number of models leads to more rapid convergence, with the risk, however, of getting trapped in local minima and thus not finding the optimal set of parameters that best describes the observations. We have been using resampling ratios between ~50% (Valla et al., 2010; van der Beek et al., 2010) and ~90% (Glotzbach et al., 2011; Robert et al., 2011), to achieve satisfactory convergence while maintaining sufficient exploration of the parameter space. Note that to take full advantage of multi-processor or multi-core technology, PECUBE has been parallelized (using calls to MPI libraries) to perform the NA sampling stage. This means that numerous forward model runs can be performed simultaneously on different processors/cores, allowing to run inversions on a high-performance cluster within a reasonable time period, typically a few days.

In early implementations of the coupled PECUBE-NA inversion, which only used the NA sampling stage (Braun and Robert, 2005; Braun and van der Beek, 2004; Herman et al., 2007), the misfit or objective function, Φ , was defined as the square root of the L_2 -norm of the weighted difference between the observed ($\alpha_{i,dat}$) and predicted ($\alpha_{i,mod}$) ages:

$$\Phi = \frac{1}{N} \sqrt{\sum_{i=1}^N \frac{(\alpha_{i,mod} - \alpha_{i,dat})^2}{\sigma_i^2}} \quad (8)$$

where N is the number of data points (thermochronological ages or fission-track length values), $\alpha_{i,mod}$ and $\alpha_{i,dat}$ are the predicted and observed ages for data point i , respectively and σ_i is the uncertainty on the data.

In the current version of PECUBE, the default misfit function has been redefined as

$$\Phi = \frac{1}{N-p-1} \sum_{i=1}^N \frac{(\alpha_{i,mod} - \alpha_{i,dat})^2}{\sigma_i^2} \quad (9)$$

where p is the number of model parameters. It has the advantage of being readily interpretable: $\Phi < 1$ means that, on average, the model

fits the data within the analytical error. However, it is not ideal for the NA appraisal stage, which requires an assessment of the likelihood of different model predictions. It is recommended to use a misfit function of the form:

$$\Phi = \sum_{i=1}^N \left(\frac{\alpha_{i,mod} - \alpha_{i,dat}}{\sigma_i} \right)^2 \quad (10)$$

which is the χ^2 statistic and from which the log-likelihood function ($\log(L)$) can be readily derived:

$$\log(L) = \sum_{i=1}^N \left(\frac{\ln(2\pi)}{2} + \ln(\sigma_i) + 0.5 \left(\frac{\alpha_{i,mod} - \alpha_{i,dat}}{\sigma_i} \right)^2 \right) \quad (11)$$

Noting that the first two terms are constant (for a given set of observations), this expression reduces to Eq. (10). Each of these expressions (8, 9 or 10) for the misfit can be selected in PECUBE.

Although the NA sampling stage is a powerful tool to extract optimal tectono-geomorphic scenarios (and/or thermo-kinematic parameters), it is not straightforward to evaluate results from a NA inversion in terms of scenarios that are allowed by the data. To derive quantitative constraints on parameter resolution, we have started to generalize the use of a companion (but independent) code (Campani et al., 2010; Herman et al., 2010a,b; Valla et al., 2010; van der Beek et al., 2010; Robert et al., 2011; Valla et al., 2011, 2012; Glotzbach et al., 2011). This second stage in the inversion procedure, called the NA appraisal stage, uses the ensemble of models generated in the sampling stage to derive posterior probability distributions of parameter value probabilities, i.e. a marginal probability density function (PDF), from the likelihood function defined above (Sambridge, 1999b). Although the log-likelihood function (Eq. (11)) is not straightforward to interpret in terms of individual model fit, it allows to statistically derive quantitative estimates of individual parameters. Modeling results can thus be represented both as scatter plots for different parameter combinations (NA sampling stage) and as 1D or 2D marginal PDFs of individual parameters (NA appraisal stage) providing quantitative details of the data resolution, i.e., the extent to which exhumation scenarios, relief evolution, and/or crustal parameters are constrained by the thermochronological data. Note, however, that model predictions are dependent on the inverse problem setup and outcomes regarding tectono-geomorphic histories are influenced by both the PECUBE and NA parameterization. Several examples of this approach will be described below.

The inverse procedure (PECUBE + NA approach as described above) requires defining both exhumation/relief scenarios and prior ranges for thermo-kinematic parameter values. The exhumation/relief scenarios are defined as a number of phases with associated exhumation rates, timing (beginning and end of the phase), and relief parameters. A main unknown in inverse theory is the appropriate dimensionality of the problem (the number of parameters that can be inverted for; e.g. Akaike, 1974; Schwarz, 1978) compared to the intrinsic resolution of the data. In general, there is a trade-off between resolution and uncertainty: whereas the fit to the data generally increases with model complexity, so does the uncertainty. One thus needs to find a balance between satisfactorily fitting the thermochronology data and over-interpreting them with too complex and geologically unrealistic models. The Bayesian Information Criterion (BIC; Schwarz, 1978) provides a way to assess the appropriate model complexity (number of parameters) allowed by the data (Gallagher et al., 2005; Glotzbach et al., 2011):

$$BIC = -2\log(L) + k\log(N) \quad (12)$$

where $\log(L)$ is the log-likelihood function (Eq. (11)), and k and N are the number of free parameters (denudation rates, timing, relief and thermo-kinematic parameters) and observations (thermochronology

data), respectively. The optimal scenario, as defined by the *BIC*-value, will thus be obtained by searching for parameter values and combinations leading to minimum misfit values for each scenario, and associated minimum *BIC* values between scenarios of different complexity (number of parameters; Glotzbach et al., 2011). Note that this approach assumes a unique maximum likelihood that explains the observed data and does not consider multiple “best-fitting” model parameterizations. However, the *BIC* approach allows the user to quantify how pertinent the choice of the preferred scenario is by evaluating the differences in *BIC*-value between several a-priori parameterizations (e.g. Valla et al., 2012).

4.1. Inversion Example 1: A synthetic problem

4.1.1. Problem setup

To illustrate the inversion procedure described above, we first present results from a synthetic study originally reported in Valla et al. (2010). The motivation for this study was to invert a synthetic age dataset (i.e., produced by a PECUBE forward-model run) to estimate how well the inversion procedure (NA) can retrieve the known model input parameters describing a well-defined relief and exhumation scenario, and thereby to test how much information on relief evolution is actually contained in a thermochronological dataset. A synthetic 2D sinusoidal topography with a wavelength of 20 km and relief amplitude of 4 km (Fig. 3A) was used to predict synthetic thermochronological data along an age-elevation profile (Fig. 3). A synthetic exhumation scenario that simulated both regional

exhumation and local relief increase was chosen in order to assess the sensitivity of the numerical approach in constraining both from a thermochronological data. We thus considered ages predicted from a model run performed over 30 Myr with a two-phase scenario (Valla et al., 2010): (1) a first phase with an exhumation rate of 0.2 km/Myr (E_1) and flat topography (the initial landscape is a plateau at the maximum present-day elevation) that ends 4.8 Myr ago (T); and (2) a second phase with similar exhumation rate ($E_2 = 0.2 \text{ km/Myr}$) but during which the relief is progressively carved to end up at the present-day configuration (Fig. 3A). In PECUBE, relief evolution is parameterized using sets of parameters, R_i and \bar{h}_i , that are defined at predetermined times in the past, t_i , such that topography, $h_i(x,y)$, at time t_i is given by:

$$h_i(x,y) = \bar{h}_i + R h_0(x,y) \quad (13)$$

where $h_0(x,y)$ is the assumed present-day topography. R_i is called the topographic amplification or relief parameter and \bar{h}_i is an offset factor. The value $R_i = 0$ corresponds to a flat topography; if $R_i < 1$ relief at time t_i is smaller than present-day; if $R_i = 1$ there has been no relief change. In the example shown here (Valla et al., 2010, from), we assumed a one-stage scenario, characterized by an arbitrary value for R between 0 and 2, and an initial offset factor equal to the maximum value of the final topography. Thermo-kinematic input parameters for these models are given in Table 1.

We used the above exhumation/relief scenario to predict synthetic low-temperature thermochronological datasets (see Valla et al.

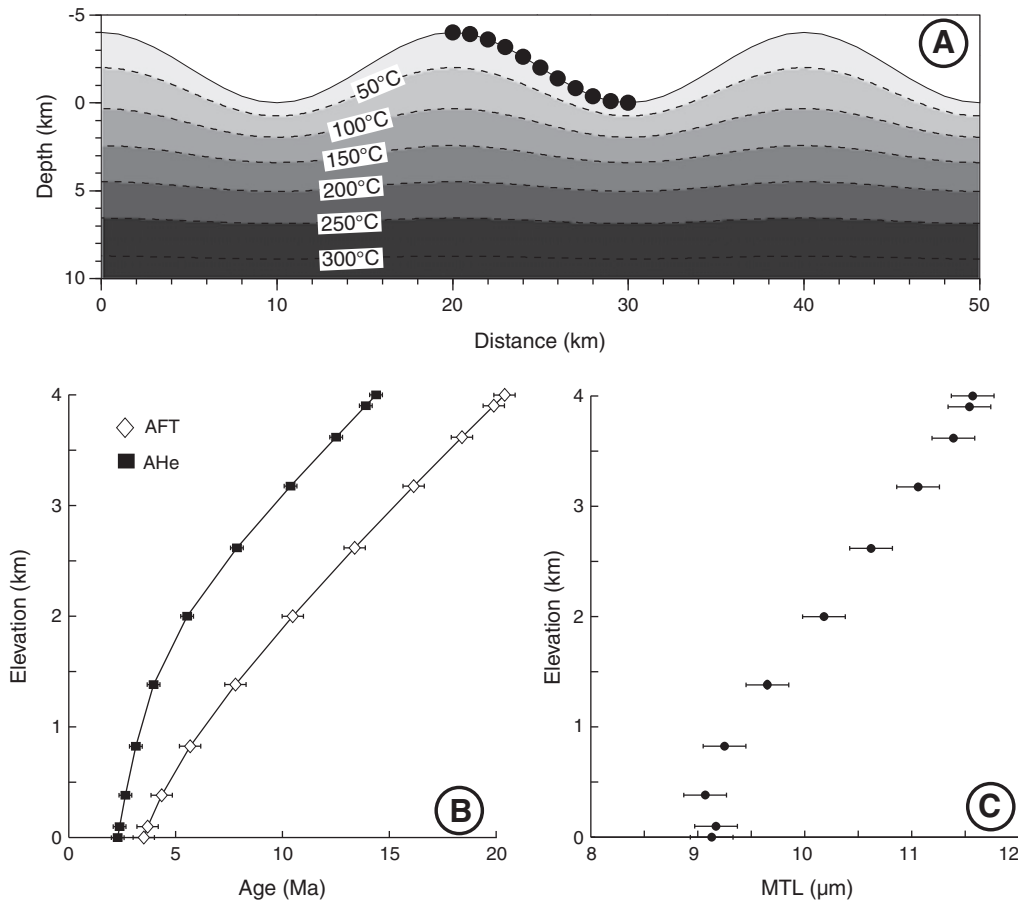


Fig. 3. Synthetic thermochronological data used for the inverse modeling. (A) Model thermal structure for a steady-state sinusoidal topography with wavelength $\lambda = 20 \text{ km}$, amplitude $A = 4 \text{ km}$ and a constant 1 km/Myr denudation rate (see Table 1 for other thermo-kinematic parameters used in PECUBE). Black circles denote synthetic samples collected along an elevation profile. (B) AFT and AHe ages versus elevation (error bars of $\pm 0.5 \text{ Ma}$ for AFT and $\pm 0.3 \text{ Ma}$ for AHe). Linear regression on the age-elevation relationships leads to apparent exhumation rates of 230 m/Myr (AFT) or 310 m/Myr (AHe) for an input rate of 200 m/Myr . (C) Mean fission-track length (MTL) versus elevation (error bars are $\pm 0.2 \mu\text{m}$). Modified from Valla et al. (2010).

Table 1

Typical thermo-kinematic and elastic parameters used in PECUBE. Crustal thickness and basal temperature are set to obtain a geothermal gradient of 25 °C/km. Poisson's ratio, Young modulus and equivalent elastic thickness are used for calculating the isostatic rebound in response to relief change. Equivalent elastic thickness is set to a value that simulates moderate isostatic rebound. Note that this particular set of parameters does not include crustal heat production.

After Valla et al. (2010).

Parameter (units)	Value
Crustal density (kg/m^3)	2700
Sublithospheric mantle density (kg/m^3)	3200
Equivalent elastic thickness (km)	25
Young modulus (Pa)	1×10^{11}
Poisson's ratio	0.25
Crustal thickness (km)	20
Thermal diffusivity (km^2/Myr)	25
Basal crustal temperature (°C)	520
Sea-level temperature (°C)	15
Atmospheric lapse rate (°C/km)	6
Crustal heat production (°/Myr)	0

(2010) for full details on thermochronological data predictions): apatite fission-track and (U-Th)/He ages (AFT and AHe ages respectively, Fig. 3B) and mean fission-track lengths (MTL, Fig. 3C). The predicted AFT and AHe age-elevation relationships (AER) are close to linear ($r^2 \approx 0.95 - 0.99$, Fig. 3B), and AER slopes suggest apparent exhumation rates of 230 m/Myr (AFT) to 310 m/Myr (AHe), i.e. overestimating the input exhumation rate ($E_1 = E_2 = 0.2 \text{ km}/\text{Myr}$). This overestimation can be explained by the additional (and spatially variable) exhumation rates induced by relief carving together with the disturbance of isotherms caused by this topographic evolution (e.g. Braun, 2002b). Extracting relief information in the present case may appear difficult as there is, a-priori, no independent information on exhumation and relief histories in the AERs (Fig. 3B). The MTL pattern presents a normal correlation between MTL and elevation, qualitatively indicating more recent cooling of valley-bottom samples as compared to ridge-top samples but providing no direct, quantitative information on relief development.

We applied the inverse numerical procedure described above to assess the resolution of the synthetic data in retrieving the input parameters (exhumation rates E_1 and E_2 , transition time T and relief factor R). Each parameter was assigned a specified prior range to be searched by the inverse algorithm, assuming a uniform distribution for the priors; for the regional exhumation rates: $E_1 \in [0 - 1] \text{ km}/\text{Myr}$; $E_2 \in [0 - 1] \text{ km}/\text{Myr}$; for the transition time: $T \in [0 - 30] \text{ Ma}$; and for the relief factor: $R \in [0 - 2]$. We chose to use constant uncertainties (no random noise added to the data, for justification see Valla et al., 2010) for the synthetic ages (σ_j , Eq. (10)) of $\pm 0.5 \text{ Ma}$, $\pm 0.3 \text{ Ma}$ and $\pm 0.2 \mu\text{m}$ for AFT, AHe and MTL, respectively, to provide an equal weight on all samples for misfit calculations. We also chose to fit the mean track length (MTL) rather than the full track-length distribution for computational convenience, although the current PECUBE version allows using full track-length distributions in the definition of the misfit function.

4.1.2. Results

To assess the sensitivity of the numerical approach to the input thermochronological data, we performed four inversions using (1) AFT ages only, (2) AFT + AHe ages, (3) AFT ages + MTL, and (4) the full AFT + AHe + MTL dataset in the construction of the misfit function (for a complete description of the inversions and full discussion of results, see Valla et al., 2010). We present the results of the first inversion stage (NA sampling stage) as scatter plots of the misfit projected along 2D planes in the parameter space (Fig. 4). Fig. 4A,B suggests that using AFT ages only provides satisfying estimates for the exhumation rates (Fig. 4A): $E_1 \approx 0.15 - 0.25 \text{ km}/\text{Myr}$ and $E_2 \approx 0.1 - 0.4 \text{ km}/\text{Myr}$; ($E_{1,\text{input}} = E_{2,\text{input}} = 0.2 \text{ km}/\text{Myr}$); however, the timing (T) and relief factor (R) predictions (Fig. 4B) do not seem tightly constrained: $T \leq 5 \text{ Ma}$ and $R \leq 0.4$ ($T_{\text{input}} = 4.8 \text{ Ma}$ and $R_{\text{input}} = 0$). Adding AHe ages and MTL data (Fig. 4C,D) does not seem to provide further

constraints on the exhumation history (E_1 and E_2 , Fig. 4C); the main difference between the two inversions lies in the predictions for T , which are much more accurate when using the full dataset ($T \approx 4 - 5 \text{ Ma}$; Fig. 4D). Finally, predictions of R suggest a significant relief increase for both inversions ($R \leq 0.4$; Fig. 4B,D) although predictions underestimate the input value ($R_{\text{input}} = 0$).

These results qualitatively show the potential ability of deriving independent constraints on both exhumation and relief histories from thermochronological data using the inversion method. They also highlight the sensitivity of output results to the type and diversity of input thermochronological data; especially, in the present case, for constraining timing and relief evolution.

The main advantage of the second inversion stage (NA appraisal stage) is to move from qualitative graphical inspection of best-fitting parameter combinations (Fig. 4) toward quantitative posterior probability distributions of individual parameter values by investigating the statistical properties of the model ensemble. We present posterior PDFs of parameter values for the 4 different inversion runs in Fig. 5. The results show that satisfactory estimates for E_1 (Fig. 5A) can be obtained using only AFT ages and that they can be improved by adding more age constraints. Predictions for E_2 and T are quite similar for all inversions (Fig. 5B,C); adding AHe ages and/or MTL increases the resolution with which the exhumation rate during the second phase can be constrained (E_2) and to some extent limit the underestimation of the age of relief change (T). Finally, predictions of R (Fig. 5D) all suggest a significant relief increase ($R < 1$), although all predictions have large associated uncertainties and all underestimate the input value ($R_{\text{input}} = 0$). This result shows that relief prediction remains the most difficult parameter to constrain using "classical" thermochronology data (Valla et al., 2010, see their discussion and further sensitivity analyses on relief predictions using thermochronological data).

This synthetic study shows that inverse numerical modeling of thermochronological AER combining various thermochronometers can prove to be an efficient tool for extracting quantitative information on exhumation and relief histories in favorable circumstances, i.e. when samples are collected along a sufficient elevation range, several thermochronometers are used and MTL information exists. The use of this inversion procedure is further illustrated in several of the case examples presented in the following sections.

4.2. Inversion Example 2: Constraining relief evolution in a tectonically active area, the Southern Alps of New Zealand

4.2.1. Motivation

Constraining relief evolution in tectonically active areas is a rather difficult problem because movement along faults results not only in exhumation but also in finite horizontal tectonic transport. The latter results in translation of features of the landscape with respect to each other and, more importantly, in relative horizontal motion between rock-particles and the elements of the landscape we are trying to constrain through the thermal history of these rocks. For these reasons, the use of a numerical model that can predict the thermal effects of fault movement and complex landforms is necessary to properly capture the complex interactions between the thermal evolution of the upper crust and its tectonic-geomorphic evolution.

A good example of such a complex system are the Southern Alps of New Zealand, where convergence between the Pacific and Australian plates, combined with an anomalously wet climate, results in extremely rapid exhumation (between 8 and 10 mm/yr) together with horizontal advection of rocks (Adams, 1981; Batt and Braun, 1997). It has been suggested that because of its very rapid erosion rate, this system, which sees an average of 800–1000 m of denudation per 100-kyr glacial cycle, is ideally suited to study the relative efficiency of glacial versus fluvial erosional processes (Herman and Braun, 2006, 2008). The Southern Alps, and in particular their western flank that receives strong orographic precipitation from humid air

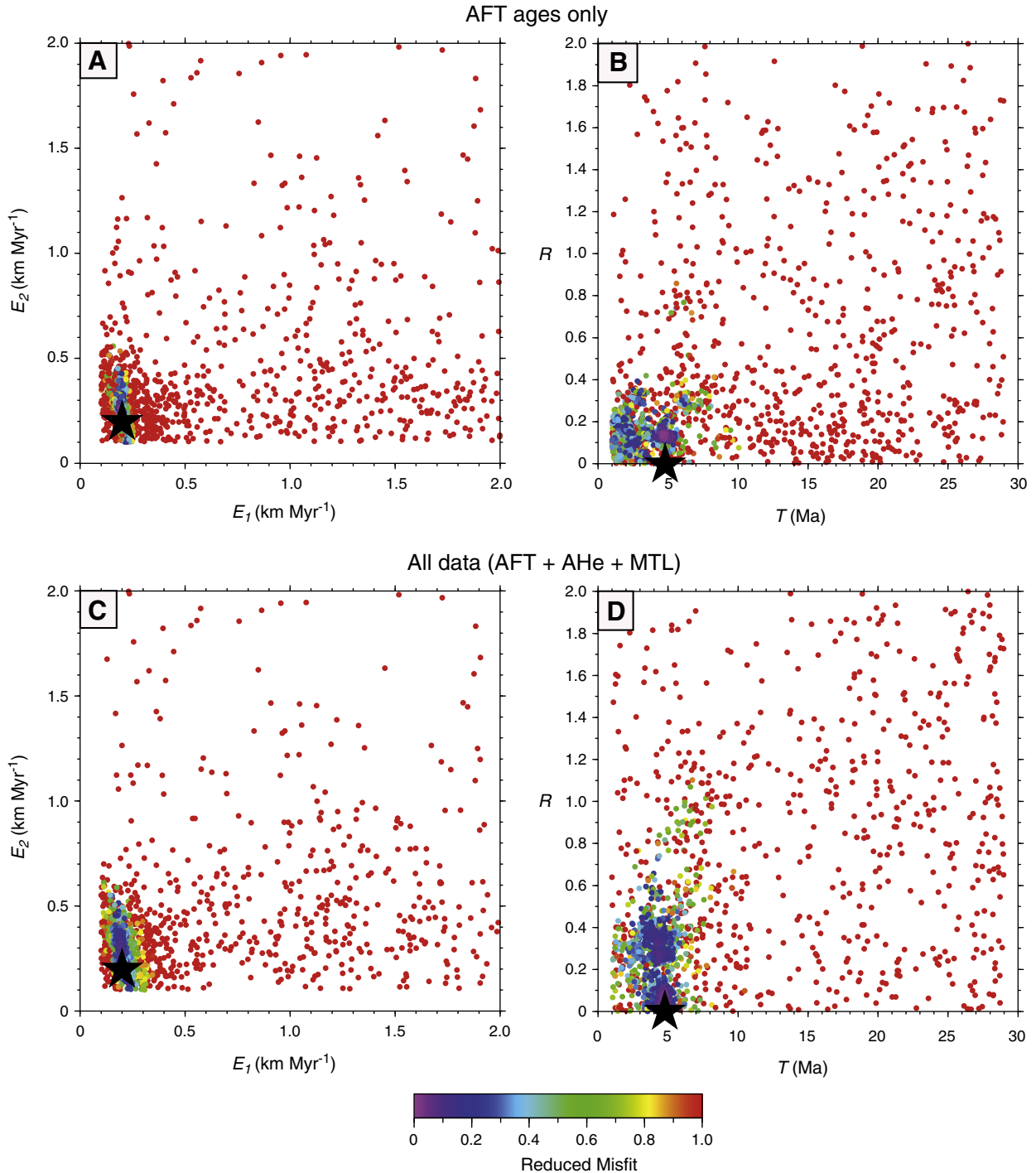


Fig. 4. Scatter diagrams showing results of the NA inversion. Each dot corresponds to a forward model; its color is proportional to the value of the reduced misfit (Eq. (8)) between predictions and the input data. Each diagram is the projection of the full parameter space onto a plane defined by two of the four parameters (denudation rates E_1 and E_2 ; transition time T and relief factor R); horizontal and vertical axes define the parameter space. Results are only shown for end-member inversions with AFT ages alone and AFT + AHe ages combined with MTL. Black stars show the “true” value of parameters used to calculate the input thermochronological data. Modified from Valla et al. (2010).

masses coming from the Tasman Sea, therefore has a unique potential to respond to climatic changes. This is further demonstrated by the rapid transformation experienced by landforms shaped by the action of fast flowing glaciers during the last glacial cycle into typical fluvial landscapes in approximately 10,000 yr (Kirkbride and Matthews, 1997).

4.2.2. A very low temperature system

The relative efficiency of glacial versus fluvial processes could be assessed by considering the relative variation in relief amplitude

that accompanies a change in the dominant erosion mechanism. Low-temperature thermochronology, with its demonstrated ability to provide quantitative estimates of relief change in favorable circumstances (Braun, 2002a; Valla et al., 2010; cf. Section 4 above) is a potentially tool to study such changes. Unfortunately, to obtain constraints on relief evolution over such a short time scale requires a very low-temperature system such that the mean thermochronological age of collected samples be of the order of the time scale over which the relief change to be quantified took place (i.e. 100 kyr). In this very

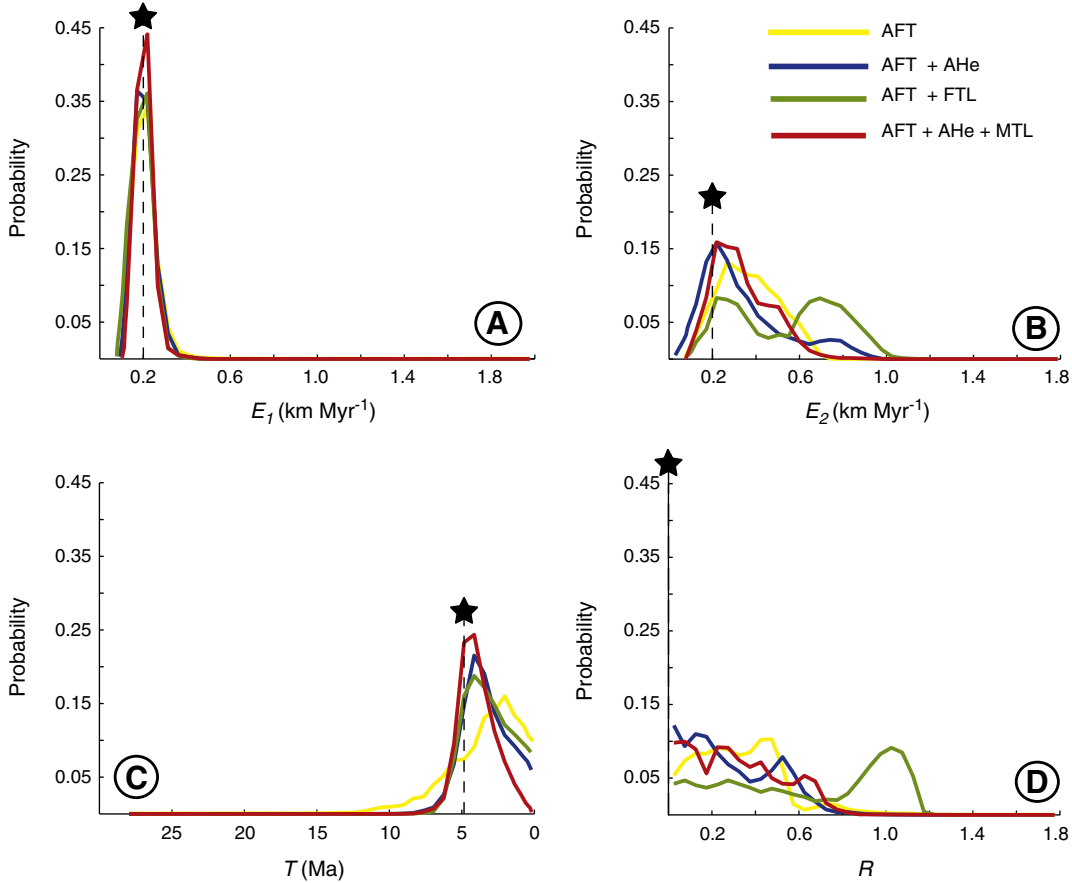


Fig. 5. 1D posterior PDFs obtained after the NA appraisal stage: (A) exhumation rate of the first exhumation phase (E_1); (B) denudation rate of the second exhumation phase (E_2); (C) transition time between the two exhumation phases (T); and (D) relief factor between the paleo-relief and the final relief (R). Each line defines an inversion experiment with a given set of thermochronological data. Vertical dashed lines and black stars represent the “true” parameter values. Modified from Valla et al. (2010).

rapidly exhuming environment, this constraint requires a system characterized by a closure temperature of a few tens of degrees at most.

Recently, Herman et al. (2010b) proposed a new very low-temperature thermochronometer that relies on the thermally activated nature of optically stimulated luminescence (OSL) in quartz and feldspar, produced by the in situ radioactive decay of K, U and Th. It is characterized by a closure temperature of approximately 30 °C and its use is limited to regions experiencing fast exhumation rate, i.e. it has an upper age limit of <1 Myr (Herman et al., 2010b). It is not the purpose of this paper to describe this new thermochronometer but to show how it can be used to estimate rates of landscape evolution on a very short times scale, as well as the special care that needs to be taken to interpret the ages it provides, in view mostly of its low closure temperature and the need to quantify all the processes that could affect the shape of the corresponding very near-surface isotherm.

4.2.3. OSL dataset to constrain recent relief change

Thirteen samples were collected along a transect in the upper reaches of the Whataroa and Perth rivers (Fig. 6A) across two major valleys that hosted large glaciers during the last glacial cycle (Herman et al., 2010b). Sampled relief is of the order of 1500 m at a wavelength of 8 to 10 km. Eleven measured OSL ages are shown in Fig. 6B (two samples did not yield a reproducible age). The mean age is about 100 ka, but large variations are observed that show some correlation with elevation along the transect (Herman et al., 2010b).

To extract a mean exhumation rate and relative relief amplitude change over the past 100 kyr, we performed an inversion of the dataset using PECUBE. Special attention was given to the surface temperature,

which was set to 0 °C during the last glacial period (this is an appropriate basal temperature for the temperate glaciers that covered the area). We assumed a geometry for the Alpine fault, the crustal-scale thrust fault accommodating most of the convergence between the Pacific and Australian plates, inferred from geophysical imaging (Smith et al., 1995), surface geology (Norris et al., 1990) and previous modeling exercises constrained by higher-temperature thermochronological data (Batt et al., 2000; Herman et al., 2009). The geothermal gradient is also relatively well constrained and known to be strongly affected by heat advection accompanying rapid rock exhumation (Batt and Braun, 1997; Shi et al., 1996; Toy et al., 2010). We used a fixed temperature at the base of the crust ($z=20$ km) of 500 °C; uniform heat production is $2 \mu\text{W}/\text{m}^3$. The inversion was constrained by the new OSL data only and three parameters were inverted for: the mean (regional) exhumation rate, the timing of hypothetical relief change and its amplitude.

The results of the inversion are shown in Fig. 7 in terms of posterior (synoptic 1D marginal) PDFs of these three model parameters. They show that the OSL data provide strong constraints on the mean exhumation rate over the past 100 kyr and that this exhumation rate is identical to estimates derived from higher-temperature systems, and thus much longer time scales (i.e. 8 km/Myr). This demonstrates that the mean exhumation rate in the central part of the South Island has remained relatively constant over a broad range of time scales. Estimates of relief change are less constrained by the OSL data but suggest that the relief amplitude, i.e. the depth of major valleys, has remained unchanged throughout the last glaciation. The timing of any relief change is unconstrained, as expected if little or no relief change took place.

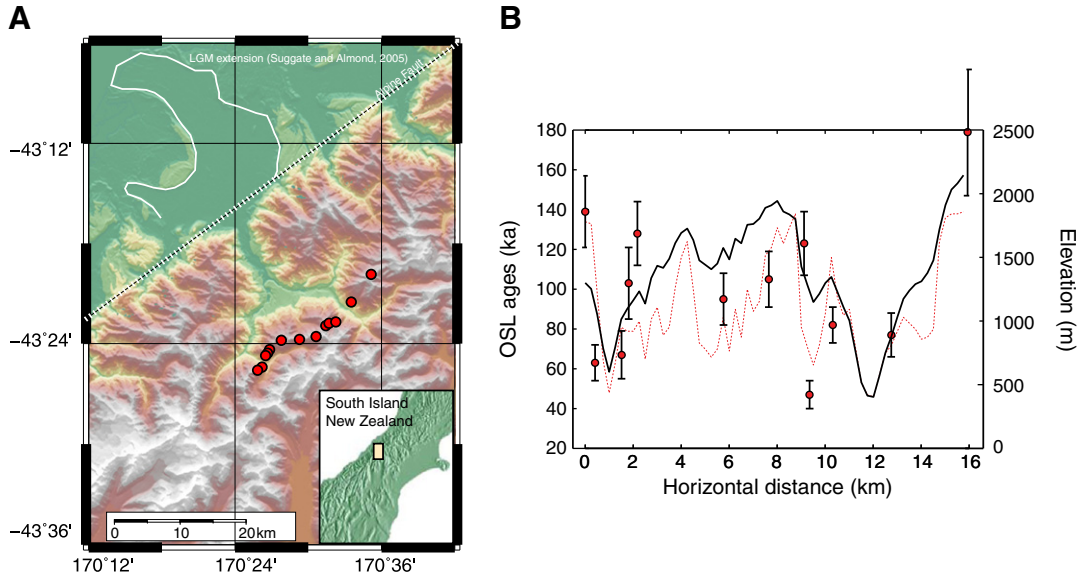


Fig. 6. (A) Digital elevation model of the Whataroa-Perth catchment in the Southern Alps, New Zealand. Red dots show the location of the OSL samples, white dashed line follows approximate surface trace of the Alpine Fault; thin white line in foreland shows extent of Last Glacial Maximum glaciers (Sugitate and Almond, 2005). Inset shows location on South Island of New Zealand. (B) Ages and elevation along the profile shown in (A). Black line is topographic profile, and red dots with error bars are measured OSL ages. Red dotted line represents the age predictions corresponding to the best fitting PECUBE model.

This relatively surprising result (there was no noticeable change in basin relief amplitude during the last glaciation) could not have been obtained by simple visual interpretation of the OSL dataset (Fig. 6B) or from the slope of local or regional AERs. High-precision modeling of the very-near-surface thermal field beneath high-amplitude and potentially rapidly varying topographic relief combined with a sophisticated inversion procedure were required to derive relief change estimates from the data, together with information on the reliability of these estimates.

5. Borehole/tunnel data

5.1. Motivation

All of the previous examples were based on thermochronology data derived from surface samples, either as age-elevation profiles along steep topographic gradients (Section 4) or as profiles across major topographic features (Section 6). The former are traditionally used to extract exhumation rates independently of knowledge on the geothermal gradient (e.g., Fitzgerald et al., 1995; Wagner and Reimer, 1972), but these estimates can be affected by the perturbation of near-surface isotherms due to topography (Braun, 2002b;

Mancktelow and Grasemann, 1997; Stüwe et al., 1994). We have shown previously (Braun, 2002b; Valla et al., 2010, and Section 4) that these effects can be extracted, under favorable circumstances, using multiple thermochronometers and inversion techniques. Thermochronology data collected along horizontal profiles crossing long-wavelength topography together with steep elevation profiles can yield important information about paleo-relief (e.g. Braun, 2002a; Ehlers et al., 2006; Herman et al., 2010b; House et al., 1998). In both cases, sub-surface samples, if accessible, can be extremely helpful to strengthen estimates of exhumation rates and predict paleo-relief. Borehole samples are often sampled along a nearly vertical transect and will provide information on exhumation rates that is not biased by topography, as well as on paleo-geothermal gradients (e.g., Gallagher et al., 2005). Tunnel samples, on the other hand, are collected along close-to-horizontal transects and will contain inherent information about the paleo-thermal structure of the crust and therefore relief development (Foeken et al., 2007; Glotzbach et al., 2008, 2011). Below, we will demonstrate these aspects using the new version of PECUBE, which offers the possibility to predict cooling ages for sub-surface samples.

These points are illustrated in Fig. 8. Heat advection through continuous exhumation together with the presence of surface topography

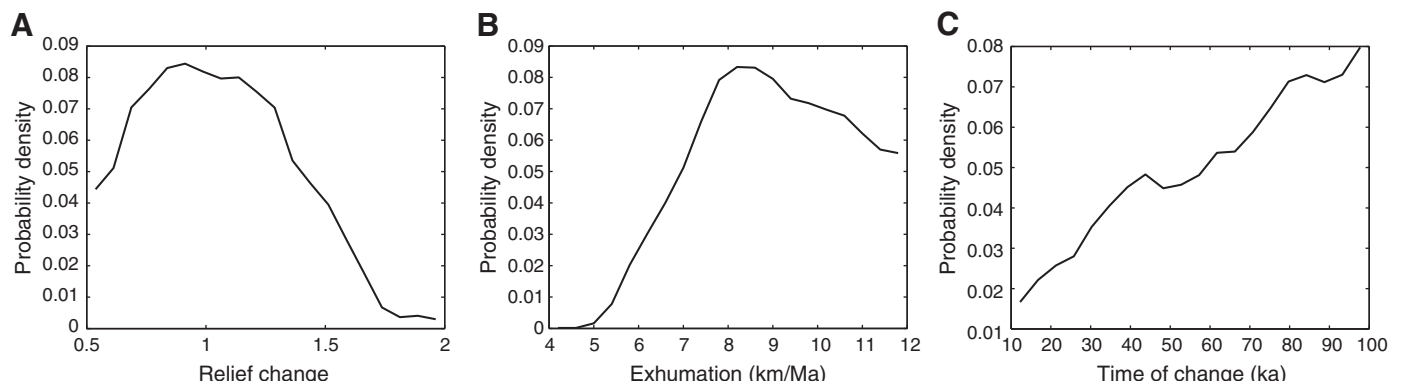


Fig. 7. Results of PECUBE inversion showing 1-D marginal integral of the PDF of (A) relief change, (B) exhumation rate and (C) timing of relief change. Note that the most probable relief change is weak ($R=1$ means no relief change) and therefore its timing is difficult to constrain. Note that 2D marginal distributions do not show any significant correlation between the model parameters.

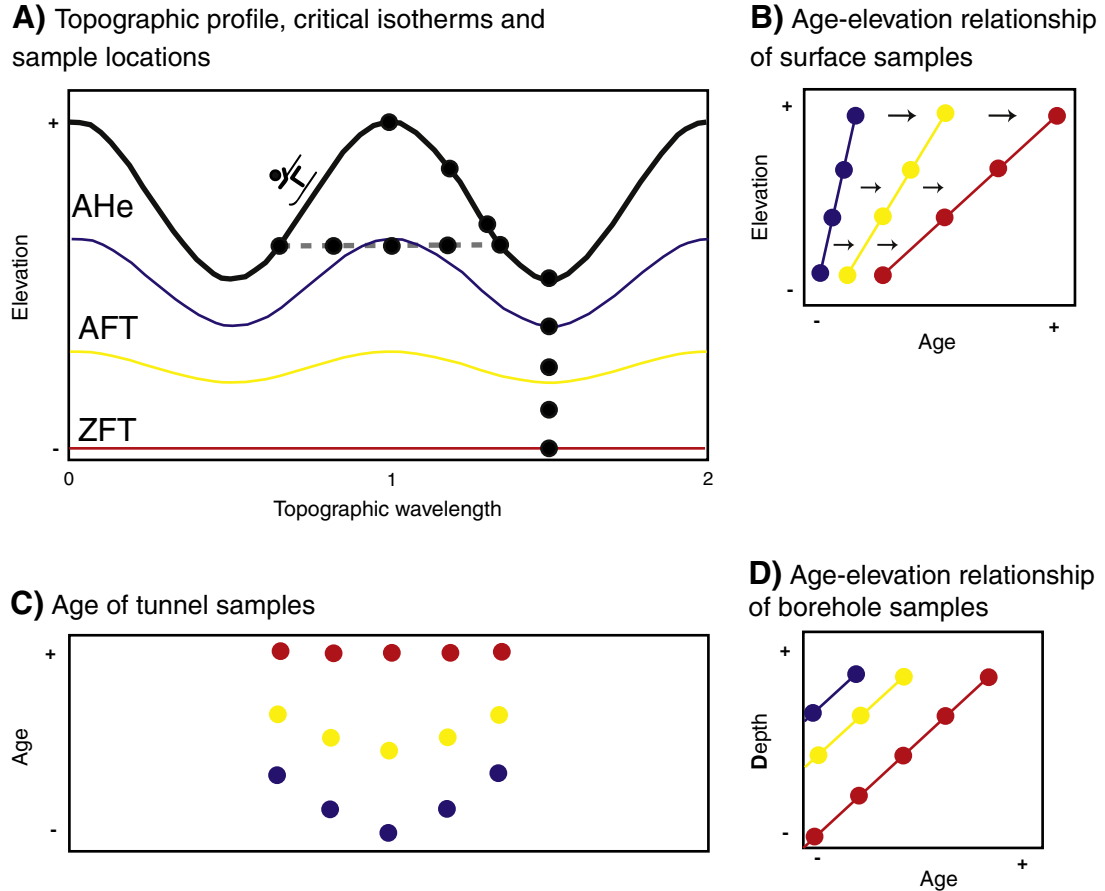


Fig. 8. Different thermochronological sampling strategies and resulting age trends. (A) Topographic profile with resulting closure-temperature isotherms for the AHe, AFT and ZFT thermochronometers. Black dots are sample locations along the surface and in a borehole and tunnel. (B) Age-elevation relationship (AER) of the AHe and AFT data are steepened due to the perturbation of isotherms; resulting exhumation rates (derived from the slope of the AER) are overestimated. The ZFT data yield the correct exhumation rates, because the corresponding isotherm is horizontal. (C) Thermochronological ages along a tunnel transect; as the ZFT closure-isotherm is not perturbed, all ages are the same. The lower-temperature AHe and AFT systems are perturbed and ages are youngest below the highest topography. (D) Borehole data; as the borehole is purely vertical, no topographic perturbation of isotherms is recorded by the data; all systems record the correct exhumation rate.

leads to perturbation of isotherms (Fig. 8A). As a consequence, low-temperature thermochronological systems such as AHe and AFT are affected. Corresponding thermochronological ages for samples taken (i) along an age-elevation profile, (ii) a tunnel transect and (iii) in a borehole are shown in Fig. 8B–D. Surface AHe and AFT ages are perturbed and, as a result, exhumation rates derived from AER are clearly overestimated (Fig. 8B). AHe and AFT ages along a horizontal tunnel transect are also perturbed (Fig. 8C), but they can be used to estimate paleo-relief. Real exhumation rates can be either derived from higher-temperature thermochronometers, in our example from the ZFT system (Fig. 8B), but only if there has been sufficient exhumation to reset those chronometers, or from vertical sample transects, such as boreholes or surface/tunnel sample pairs (Fig. 8D). Thus the combination of surface and borehole/tunnel samples avoids inaccurate interpretation of thermochronological data (e.g., overestimation of exhumation rates) and enables precise estimation of paleo-relief.

5.2. Implementation in PECUBE

As explained earlier, PECUBE predicts the thermal history of points located at the surface of the model at the nodes of the finite element grid used to solve the heat Eq. (2). The code was modified to track the location through time of any arbitrary point and, in particular, a set of points that is specified in an input file, namely points where the user will have data, i.e. cooling ages. The longitude and latitude of these points must be given, as well as their altitude with respect to mean sea level or depth (if negative number) with respect to the local

topographic surface. In addition to this information, the user must specify the location (longitude–latitude pair) of the bottom left corner of the PECUBE finite element grid, the spacing in degrees between the mesh points and the number of mesh points in both directions, if the geometry of the topographic surface is specified on a regular rectangular grid, such as provided by a DEM, or the location of each point of the topographic surface in longitude–latitude coordinates and the topology of the triangles connecting these points, if the geometry of the topographic surface is specified on a set of arbitrary points. The computation of temperature histories for these arbitrarily located points was easily implemented in PECUBE as, following the implementation of complex fault geometries, particle points move along trajectories that are not vertical and must therefore be tracked in full 3D geometry. This is explained in greater detail in Section 6.

5.3. Synthetic dataset

To quantify the error associated with the interpretation of surface samples alone and the improvement obtained by considering subsurface samples, a synthetic thermochronological dataset has been produced using PECUBE for a periodic topography (similar to that in Fig. 3A) with a wavelength of 20 km and a relief of 2 km (Fig. 9A). AFT and AHe ages were calculated for surface, borehole and tunnel samples for steady-state topography and an exhumation rate of 1 km/Myr from 40 to 5 Ma, followed by a period of reduced exhumation rate of 0.1 km/Myr after 5 Ma.

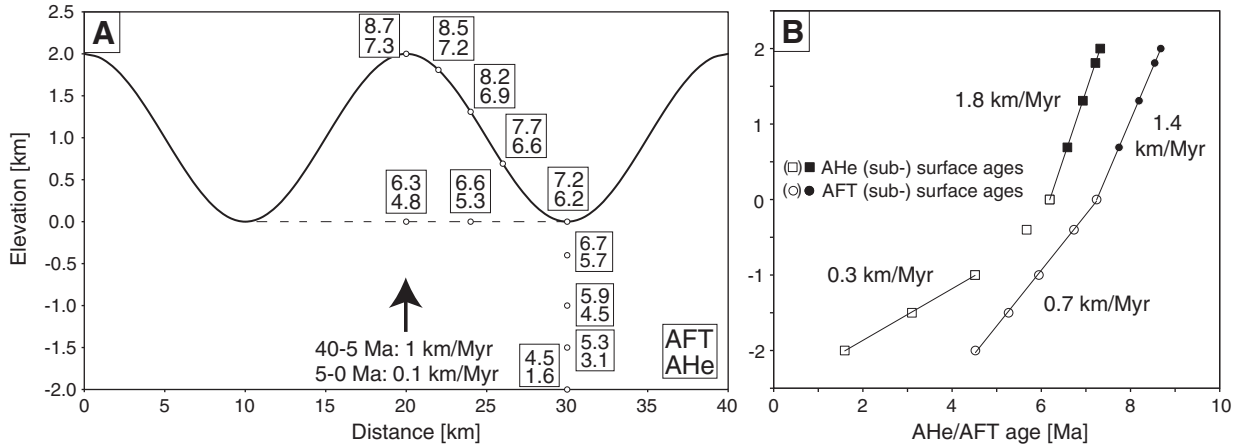


Fig. 9. Synthetic AHe and AFT ages calculated with PECUBE for steady-state topography with a wavelength of 20 km and a relief of 2 km. Model exhumation rates were spatially constant at 1 km/Myr for the first 35 Myr followed by 5 Myr of slow exhumation, at 0.1 km/Myr. Other input parameters are as follows: AHe diffusion and AFT annealing models of Farley (2000) and Ketcham et al. (1999), respectively; temperature at the base of the model (30 km) of 600 °C, temperature at sea level of 10 °C, atmospheric lapse rate of 5 °C/km, no heat production. (A) Topographic profile, sample locations and modeled AHe and AFT ages. (B) AER of AHe (squares) and AFT (circles) ages for surface and borehole samples, with slopes fitted to subsets of the data that are linearly aligned.

The predicted ages and locations of the synthetic sampling sites are shown in Fig. 9A. The resulting AER are shown in Fig. 9B and demonstrate that correct estimates of the mean exhumation rate and the time at which it changed cannot be retrieved from casual inspection of the AER alone. Even though sub-surface samples have been collected, none of the exhumation rates derived from the slope of the AER is correct: exhumation rates derived from surface samples alone are overestimates due to the topographic perturbation of isotherms, and exhumation rates derived from AER of borehole samples are affected by the transient downward migration of isotherms in response to the decreased exhumation rate. Not only are exhumation rates incorrect, but neither can the time of change in exhumation be accurately derived from this simple 1D interpretation: the break-in-slope indicating the change in exhumation rate appears to be older than the time of actual change in exhumation rate. This effect is due to the relatively sluggish nature of heat conduction in the Earth's crust, leading to a thermal response time of several Myr to changes in exhumation rate. Thus, in general, simple 1D interpretation of AER is not suitable to resolve transient features of a topographic or exhumational history. We show now that numerical 3D thermal modeling (e.g. using PECUBE) needs to be applied to find reliable exhumation/relief scenarios that fit the observed data.

In the following, Neighborhood Algorithm (NA) inversions (see Section 4) were applied to efficiently search exhumation/relief parameter combinations that fit the synthetic thermochronological data. Model setup and parameter bounds were chosen to encompass the known parameter values (cf. previously described model setup), and all inversions comprised five free parameters: (1) a topographic amplification factor and (2) time of onset of relief change, (3) initial exhumation rate since 40 Ma, (4) time of change in exhumation

rate and (5) new exhumation rate. Three inversions were conducted using only five out of the eleven synthetic samples shown in Fig. 9 to simulate different sampling strategies. Inversion results are shown and compared in Fig. 10 and Table 2.

In general, parameter estimates derived from NA inversions fit “real” (input) values better when incorporating sub-surface samples. As for the AER-derived estimates, optimal parameter values based on inversion of surface samples only overestimate exhumation rates and poorly fit the time of exhumation change. Including borehole or tunnel samples significantly increases the accuracy of the inversion estimates (Fig. 10, Table 2). Note that although all synthetic ages were produced with a steady-state topography (corresponding to a relief amplification factor of 1), most of the inversions predict significant relief change. The inversions suggest relief amplification factors of 0.6 ± 0.3 (surface samples), 0.75 ± 0.20 (surface/borehole samples) and 0.85 ± 0.15 (surface/tunnel samples) at the time when tunnel samples cooled through the AFT and AHe closure temperature (i.e., ~ 6.5 and ~ 5 Ma, respectively). This shows that surface samples alone may be insufficient to reliably predict exhumation or relief evolution (see also Valla et al., 2010, and Section 4), but that the combination of surface and sub-surface samples, in particular from tunnel transects, can be used together with 3D numerical thermal-kinematic modeling (e.g., PECUBE) to yield more accurate estimations of exhumation and relief evolution.

5.4. Example: Mont Blanc tunnel transect

Recently, several studies have reported thermochronological data collected along tunnel transects and their corresponding surface traces to reconstruct exhumation histories and estimate paleo-relief

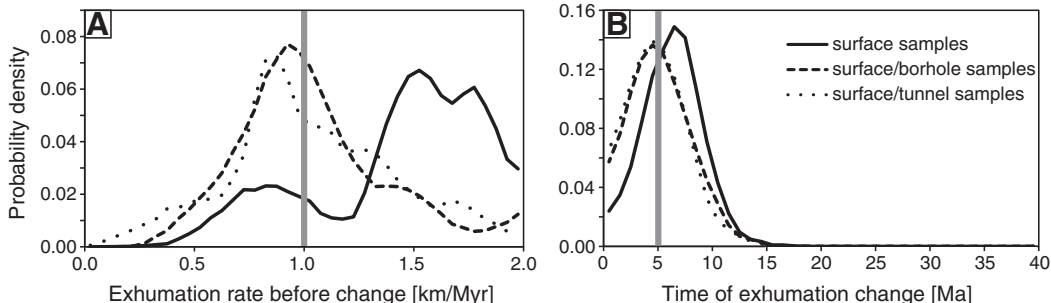


Fig. 10. 1D marginal probability plots of the initial exhumation rate (A) and time of exhumation change (B) predicted for different sampling strategies. Means and standard errors of all free parameters are shown in Table 2. The gray vertical line shows the input parameter value for each plot.

Table 2

Mean and standard error of free parameters inferred from NA inversions of different sub-sample sets and corresponding input values.

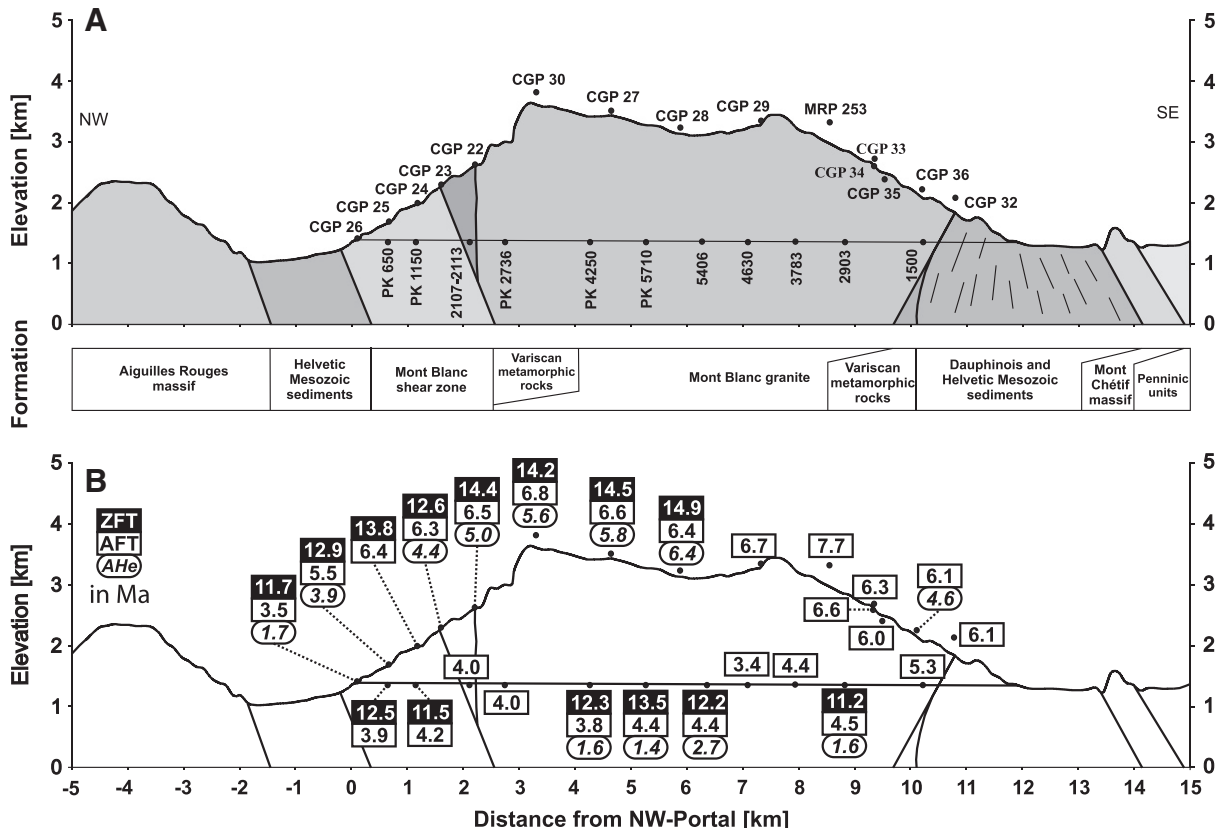
	Unit	Forward model	Surface samples	Surface/borehole samples	Surface/tunnel samples
Time of topography change	Ma	–	18 ± 8	24 ± 12	21 ± 12
Topographic amplification factor	–	1	0.33 ± 0.27	0.37 ± 0.28	0.62 ± 0.21
Exhumation rate 1	km/Myr	1	1.4 ± 0.4	1.0 ± 0.3	1.0 ± 0.3
Time of exhumation change	Ma	5	6.3 ± 2.7	5.2 ± 2.8	5.0 ± 2.7
Exhumation rate 2	km/Myr	0.1	–0.3 ± 0.4	0.1 ± 0.4	0.0 ± 0.5

(Foeken et al., 2007; Glotzbach et al., 2008). One of these studies sampled the Mont Blanc tunnel (Glotzbach et al., 2008), crossing the Mont Blanc external crystalline massif in the Western Alps (Fig. 11). Sampling strategy and present-day relief are comparable to the previous synthetic model setup; however, the measured thermochronological age pattern is slightly different (Figs. 10 and 11). Note, in particular, the uniformity of AHe and AFT ages along the tunnel, which has been interpreted to imply a significant recent increase in relief (Glotzbach et al., 2008).

Based on the results from a qualitative interpretation of the dataset (Glotzbach et al., 2008), inverse PECUBE modeling was used to better quantify the Neogene exhumation and relief history of the Mont Blanc Massif. The approach is similar to the one presented in Section 4, with the Bayesian Information Criterion used for optimal model (parameter) selection (Schwarz, 1978). With the objective of finding the most probable exhumation scenario, a first set of inversions was performed assuming steady-state topography. Results suggested that a three-step exhumation scenario best explains the data with acceptable model complexity. Corresponding exhumation paths are shown in a synoptic 2D marginal probability density function (PDF) in Fig. 12A. These results support a scenario in which exhumation of the Mont Blanc massif was

episodic, with a drop in exhumation rate at 6 ± 2 Ma, followed by a dramatic increase at 1.7 ± 0.8 Ma.

There is independent evidence that the late increase in exhumation is linked to climate change, with initiation of major glaciations leading to efficient valley incision and deepening (e.g., Haeuselmann et al., 2007; Hinderer, 2001; van der Beek and Bourbon, 2008). To test this hypothesis, we performed a second set of inversions that included the possibility of relief increase. The relief scenario assumes, for simplicity, that paleo-topography evolved linearly between the initial topography before glaciation started (characterized by the relief ratio R ; cf. Section 4) and the present-day topography. Results of the inversion shown in Fig. 11 suggest that the most probable scenarios are characterized by an approximate doubling in relief ($R = 0.5 \pm 0.1$) starting at 0.9 ± 0.8 Ma (Glotzbach et al., 2011), and a consequent increase in local (but not regional) exhumation rate at the same time (Fig. 12B–D). Resulting misfits are comparable to a scenario with steady-state topography, but clearly the tunnel data are better accounted for with the second model setup; the misfit values (as defined by Eq. (10)) being respectively 106 and 59. This better fit to the sub-surface data and the more reasonable exhumation histories, together with the correspondence between the timing of predicted relief increase in the Mont



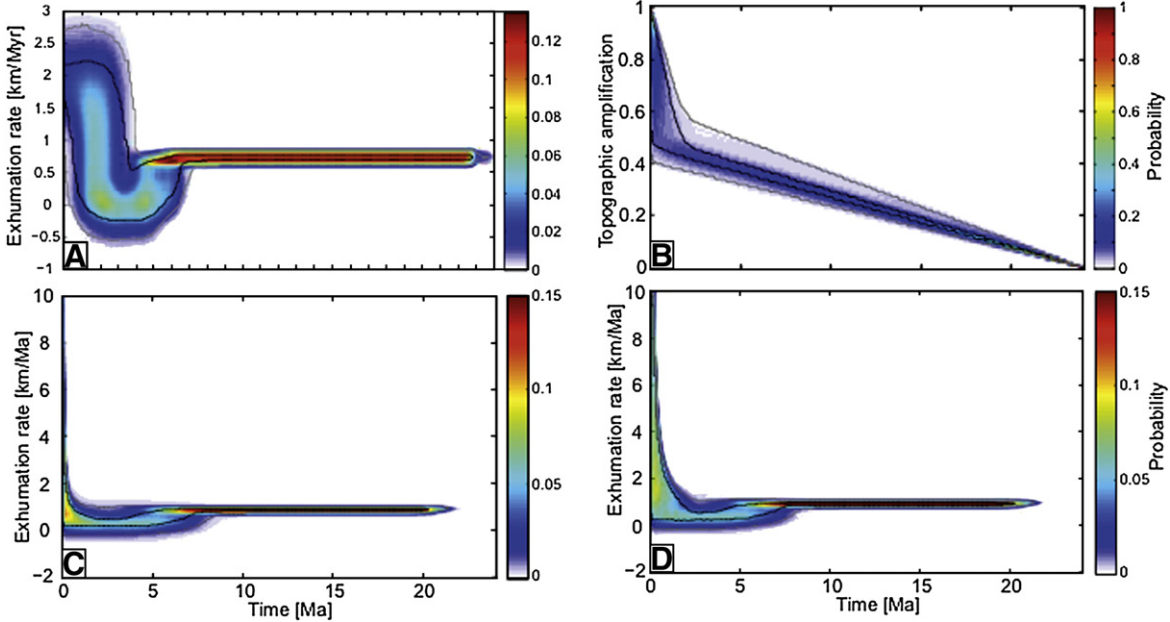


Fig. 12. Synoptic 2D marginal PDF of exhumation and relief evolution path of the Mont Blanc massif. Probabilities and corresponding 2σ (gray) and 1σ (black) confidence intervals are constructed using re-sampling of the dataset (cf. Section 4). (A) Most probable exhumation scenario assuming steady-state topography. (B–D) Most probable relief evolution (B) and exhumation paths for models including relief change. Total exhumation histories (i.e., including both regional exhumation and local valley carving) are exemplified for a ridge (CGP30 at 3750 m; C) and valley (CGP26 at 1277 m; D) sample, respectively.

Blanc massif and elsewhere (Haeuselmann et al., 2007; Valla et al., 2012) with the initiation of major glaciations at 0.87 Ma (Muttoni et al., 2003), lead us to prefer the relief scenario and to suggest that valley glaciers have markedly increased the relief in the western Alps in the last 1 Myr (Glotzbach et al., 2011).

6. Faulting

6.1. Motivation

In active orogens, shortening is accommodated by motion along reverse faults that results in rock advection in both horizontal and vertical directions. The vertical advection of rocks results in a strong perturbation of the thermal structure of the crust, which has to be taken into account when interpreting thermochronological data (Batt and Braun, 1997; Ehlers and Farley, 2003). The horizontal component, in turn, may lead to other complexities resulting from cooling of rock samples that are currently closely spaced in different thermal fields, often separated by large horizontal distances (Batt and Brandon, 2002). In this way, offsets in age distributions are often interpreted as resulting from differential exhumation across a fault (Kohn et al., 1999; Fitzgerald et al., 1999; Bermúdez et al., 2011).

In the initial version of PECUBE, only vertical advection of material (and heat) was considered. To be able to test hypotheses concerning the presence or timing of motion along faults and their implications on observed thermochronological datasets, we implemented a module that considers the thermal effect of rock motion along one or more faults. In PECUBE, cooling ages are derived from the time–temperature history of particles that end up at the surface of the model (representing the present-day situation), which requires tracking the position of each of these particles throughout the model run. This is performed by using a three-dimensional velocity field that represents rock motion through time. To represent rock motion associated with displacement along a fault, we use a variation of the kink-band model originally developed by Braun et al. (1994) to represent the deformation of the hanging wall along a listric normal fault. A complete description of the velocity field used is given below.

6.2. Definition of faults in PECUBE

6.2.1. Reference frame

The definition of a fault requires two sets of parameters. The first specifies the geometry of the fault and the second defines the velocities of the two blocks on either side of the fault. The easiest way to define a fault and to track the time–temperature path of particles that form the present-day surface is to use the fault as a reference frame, i.e. the fault is assumed to be fixed with respect to an external reference frame and to the topography. This choice is made for computational efficiency. It is clear that one of the two crustal blocks (or both) on either side of the fault will move with respect to the fault; however in its present form, PECUBE does not allow for advection of the surface topography, i.e. the shape of the surface is not advected even if all or part of the surface rocks move with respect to the reference frame. One way to justify this choice is to consider that surface processes are always sufficiently efficient to maintain the shape of the topography in a steady-state configuration, regardless of horizontal tectonic advection. It is clear, however, that this remains an approximation.

6.2.2. Fault geometry

We first consider how the geometry of a single fault has been incorporated in PECUBE. The fault geometry is defined in a local coordinate system (r,s) that is different from the global three dimensional coordinate system (x,y,z) in PECUBE. As shown in Fig. 13, this system is fully defined by the position in the global coordinate system of two points $A(x_1,y_1)$ and $B(x_2,y_2)$ in the horizontal plane at $z=z_l$, where z_l is the surface of the model, as defined in PECUBE. The r -axis of the fault coordinate system is located to the right of that line (when moving along the line from point A to point B), the s -axis is vertical and the origin is located anywhere along the line at $z=z_l$. This definition of the origin implies that the fault geometry is in fact two-dimensional; the fault is “expanded” laterally along the line defining its origin.

In the vertical (r,s) plane, a series of n connected points (r_i,s_i) defines the fault trace in the (r,s) plane corresponds to the segments connecting the points (r_i,s_i) . The end segment is assumed

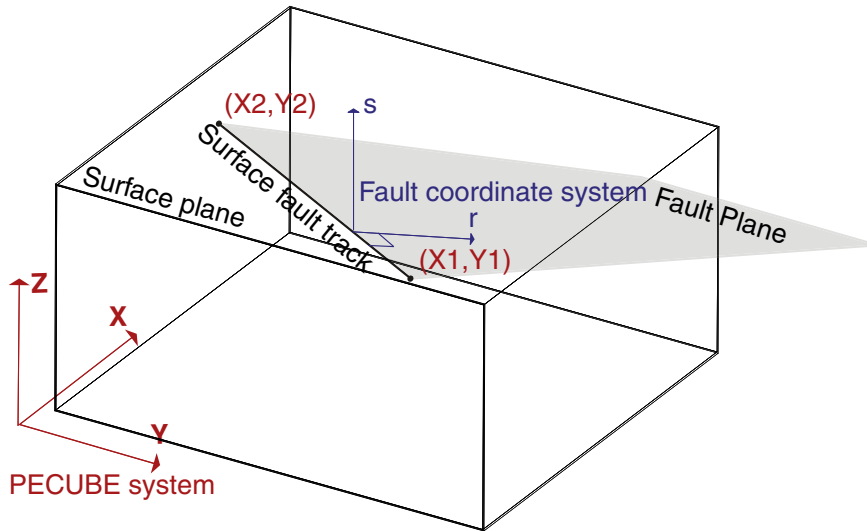


Fig. 13. Definition of fault geometry in PECUBE, using a local fault-coordinate system (r,s) and the global PECUBE system (x,y,z).

to continue indefinitely at a constant slope, defined by the last two points on the fault trace.

The fault limits two half-spaces, one on either side of the fault. The order in which the nodes are given determines which half-space moves with respect to the fault: it is the one to the right of the fault when moving along the fault-plane in the order in which the nodes are given in the input file. The other half-space is assumed to be fixed. This convention implies that to define movement of the hanging wall of a fault (dipping away from the origin line (A–B) on the surface), the points need to be defined from the deepest part of the fault to the surface ($r_i > r_{i+1}$). To define movement of the footwall, the points need to be defined from the surface to the deepest part of the fault ($r_i < r_{i+1}$). If one wishes to make the second half-space move too, one needs to define a second fault with the same geometry but with the nodes given in the reverse order.

6.2.3. Fault kinematics

The velocity across the fault, v_0 , is prescribed as an input parameter. It represents the value of the far-field horizontal velocity difference between the two blocks. The sign of v_0 defines its sense: by convention, normal faults have a positive velocity, thrust faults a negative velocity.

The two-dimensional velocity field, i.e. at every point of coordinates (r,s), is calculated from the geometry of the fault. The algorithm is rather simple and easy to implement.

First, one considers each segment individually. In the region defined by a fault segment and its normals at each end of the segment, the velocity is set parallel to the fault with amplitude v_0 . Two situations have to be considered next, when considering successive fault segments: they either form an acute (closed) or obtuse (open) angle (Fig. 14).

In the first case (acute angle), the direction of the velocity vector in the “overlapping” region is set to the mean of the directions of the two segments (using the definition of the sum of two vectors to calculate the mean); its amplitude is given by:

$$v'_0 = v_0 \frac{\cos \alpha}{\cos \frac{\alpha}{2}} \quad (14)$$

where α is the angle made by the two normals to the segments. In the second case, the direction is also the mean of the directions of the segments, but the amplitude is given by:

$$v'_0 = v_0 \frac{1}{\cos \frac{\alpha}{2}} \quad (15)$$

The amplitudes are obtained by imposing continuity of the normal component of the velocity across the boundaries defining the various regions, to ensure mass conservation.

This two-dimensional velocity field is finally rotated and translated by a simple change of coordinate system from the “local” fault system (r,s) to the “global” PECUBE system (x,y,z), using:

$$\begin{aligned} v_x &= v_r * x_n \\ v_y &= v_r * y_n \\ v_z &= v_s \end{aligned} \quad (16)$$

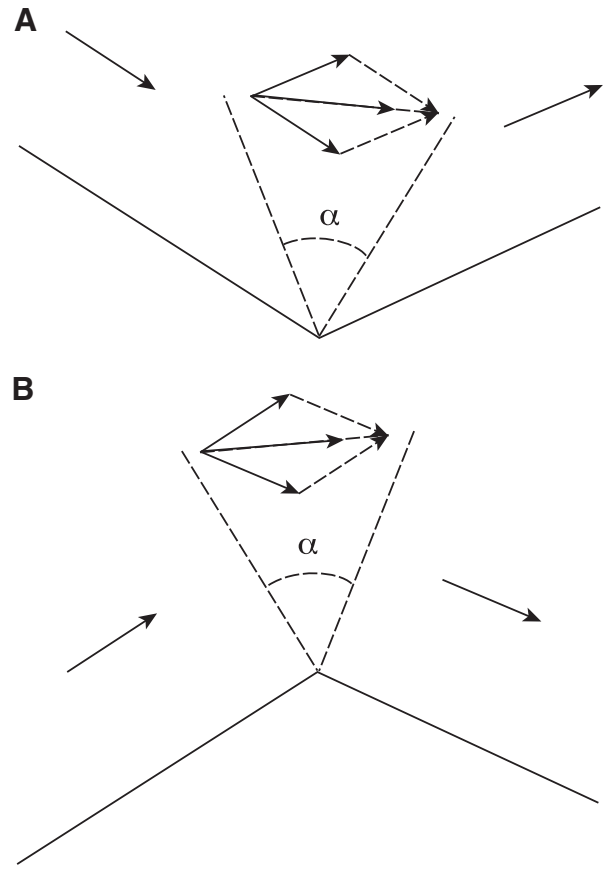


Fig. 14. Imposed velocity field in the vicinity of a kink in the fault.

where $(x_n, y_n, 0)$ are the coordinates of the unit normal to the fault trace in the global (x, y, z) system of reference.

Note that the velocity is only defined for regions falling within the strip perpendicular to the two points (x_1, y_1) and (x_2, y_2) . These points can be defined to lie outside of the modeling space such that, if the direction between the two points is oblique to the sides of the box, the velocity field can still be defined in all parts of the modeling space.

In PECUBE, one must also define the history of fault motion. This is defined by a number of time intervals (start and end times), with a velocity associated to each time interval following the sign convention outlined above.

Optionally, a friction coefficient, φ_r , can be defined to take in account shear heating along the fault (H_h). Shear heating is assumed to be proportional to the second invariant of the shear strain, $\dot{\varepsilon}$, estimated from the gradient of the velocity field:

$$\begin{aligned}\dot{\varepsilon} &= \sqrt{\sum_{ij} \dot{\varepsilon}_{ij} \dot{\varepsilon}_{ij} / 2} \\ \dot{\varepsilon}_{ij} &= \left(\frac{\partial u_i}{\partial x_j} + \frac{\partial u_j}{\partial x_i} \right) / 2\end{aligned}\quad (17)$$

and an arbitrary uniform stress value, σ_u , of 100 MPa (Molnar and England, 1990), such that

$$H_h = \varphi_r \frac{\dot{\varepsilon} \sigma_u}{pc}. \quad (18)$$

An arbitrary value of 1000 J/kg K is used for the heat capacity, c .

6.2.4. Multiple faults

Some model simulations may require the definition of several faults, moving sequentially through time and/or together during the same time interval. When considering the compounded movement of several faults, one must take into account the advection of the position (and potentially the deformation of the geometry) of faults with respect to each other. This quickly becomes an intractable problem that requires balanced restoration of the modeled cross-section (e.g., Erdos et al., 2011). In order to simplify the problem, a flag has been set to determine if the geometry of each fault remains fixed, or if it is to be updated by considering the motion along other faults.

Finally, it is worth noting that when the fault geometry is not fixed, faults are advected by considering whether they are on the ‘moving side’ of the active fault(s) and applying the corresponding displacement (product of the velocity and the time step) to each of the points defining the fault. If the fault being displaced lies within a uniform velocity field, straight segments remain straight and no deformation of the fault plane occurs. However, when the fault is displaced by a non-uniform velocity field (such as in the vicinity of a kink), the advected fault will be deformed by the non-uniform velocity field. For the fault geometry to remain acceptable, it needs to be defined by a large number of small segments.

6.3. Faulting example: Faulting sequence in central Nepal

The fault module was first developed to address the problem of timing of fault activity in the central Nepal Himalaya (Robert et al., 2009, 2011). In these papers, we explored the consequences of potential out-of-sequence faulting on thermochronological age patterns: it had been suggested in several papers (e.g. Hodges et al., 2004; Wobus et al., 2003, 2006) that the observed pattern of thermochronological ages in central Nepal required recent reactivation of the Main Central Thrust system of the Himalaya, while others (e.g. Bollinger et al., 2004, 2006) suggested that this pattern could be explained by movement over a crustal-scale ramp in the main detachment system underlying the

Himalaya, coupled with underplating. This same problem was also addressed independently by Herman et al. (2010a) using PECUBE inversions and Pecube-Cascade coupled models, who came to very similar conclusions to those outlined below.

6.3.1. Model setup

Fig. 15 shows the boundary conditions as well as the velocity field of the model developed to address the above question. The topography is extracted from the SRTM V2 digital elevation model downgraded to a resolution of 1 km. This resolution is adequate, as shown by Valla et al. (2011). We assumed the topography to be in steady state and did not attempt to extract information about topographic change from the thermochronological data. Steady-state topography has been assumed by practically all thermal-kinematic modeling studies of the central Himalaya (e.g. Brewer and Burbank, 2006; Wobus et al., 2006; Bollinger et al., 2006; Whipp et al., 2007). Moreover, Galy et al. (2010) have recently shown, using multiple isotopic data from the Bengal Fan, that the erosion patterns, drainage systems and mean elevation of the Himalaya and southern Tibetan plateau have remained relatively stable for the last 12 Myr, despite major climatic changes during this time span.

The initial model geometry is based on the inferred structure of the Main Himalayan Thrust (MHT) in central Nepal (Cattin and Avouac, 2000; Avouac, 2003; Pearson and DeCelles, 2005); i.e. a flat-ramp-flat geometry with the mid-crustal ramp located below the topographic transition between the Lesser and the High Himalaya (Fig. 15). The geometry of the crustal ramp is constrained by the slope break observed in a seismic receiver-function cross-section of the central Nepal Himalaya (Nabelek et al., 2009, and Fig. 15A) and the microseismicity pattern (Pandey et al., 1999, and Fig. 15B). The MHT is active throughout the model run and its surface trace (origin for the PECUBE models) is the Main Frontal Thrust (MFT; Avouac, 2003; DeCelles et al., 2001). Previous thermo-kinematic models for the central Nepal Himalaya have shown that, for a reference frame fixed to the MHT, observed thermochronological ages require overthrusting velocities of 5–6 km/Myr (Avouac, 2003; Bollinger et al., 2004; Brewer and Burbank, 2006; Whipp et al., 2007), implying underthrusting of the Indian plate at a velocity of ~15 km/Myr in order to obtain a total convergence rate of 20–21 km/Myr (Avouac, 2003; DeCelles et al., 2001; Mugnier et al., 2004). Here we use over- and underthrusting velocities of 6 and 15 km/Myr, respectively. We finally include a second fault representing the Main Central Thrust (MCT) that breaks to the surface at the front of the “topographic transition” between the Lesser and the Higher Himalaya (Wobus et al., 2003, 2006). We vary the velocity and timing of onset of this fault to simulate various degrees of out-of-sequence thrusting: keeping the total overthrusting velocity fixed (Fig. 15). We set the surface conductive temperature gradient at 35 °C/km, by imposing the basal temperature T_0 of 850 °C and a heat production rate (A in Eq. (2)) of 6.5 °C/km. The surface temperature is fixed at 25 °C and the thermal diffusivity at 25 km²/Myr. Models are run over a 10 Myr period. By default, PECUBE uses the conductive/advection steady-state solution corresponding to the imposed velocity field at the beginning of computation as the initial temperature condition.

To constrain the model, we used thermochronological datasets collected in the area (Bollinger et al., 2004; Herman et al., 2010a; Robert et al., 2009, 2011). Particle paths are tracked through time, using the velocity field defined by the fault geometry and kinematics described above, for rocks that end up at the surface at the end of the model run; the resulting time-temperature paths were used to predict apatite and zircon fission track ages using the fission-track annealing model of Green et al. (1989) with the modified annealing parameters of Stephenson et al. (2006) for AFT, the zero-damage model of Rahn et al. (2004) for ZFT and the standard He diffusion parameters as described in Section 3.2.

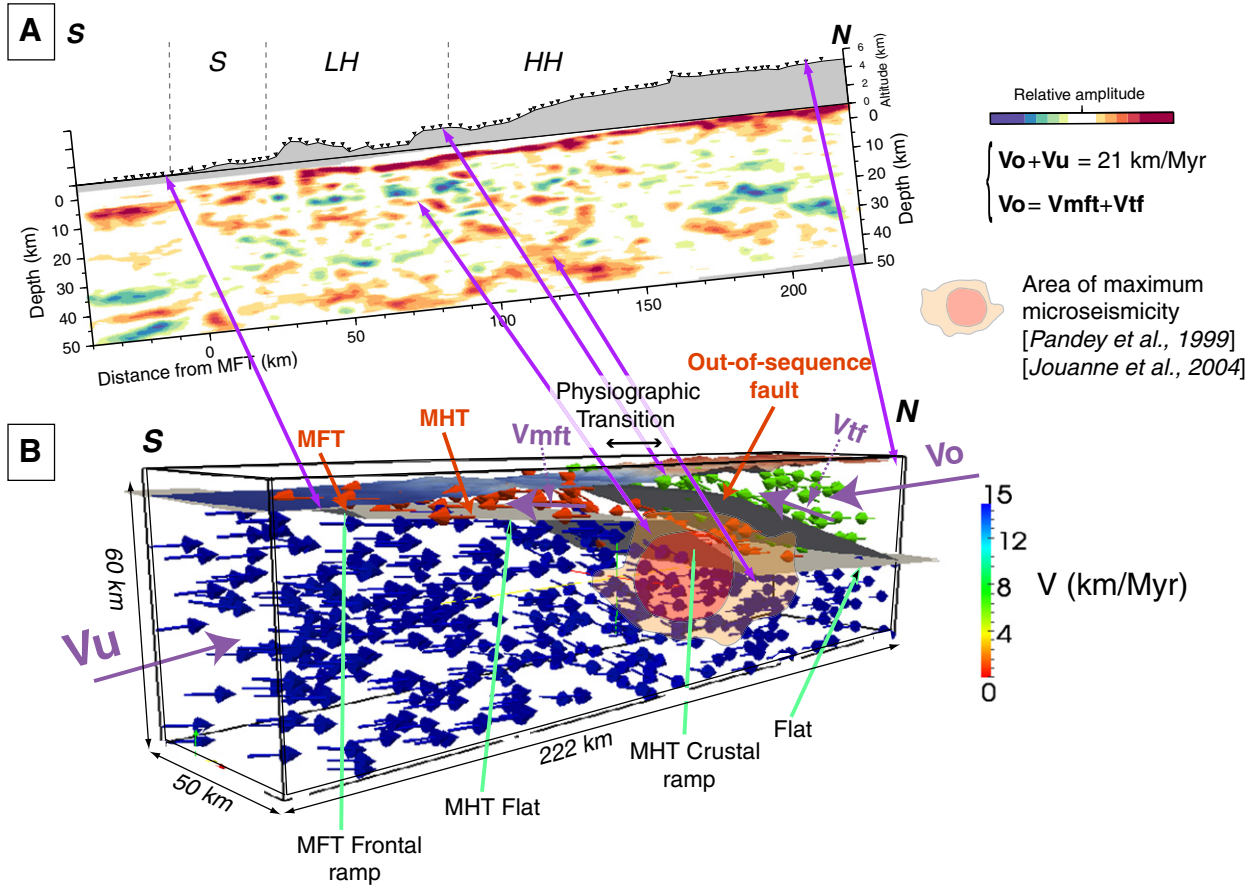


Fig. 15. (A) Receiver function image of a cross-section across the central Nepal Himalaya at 85° E, approximately at the longitude of Kathmandu (Nabelek et al., 2009). Red and blue colors represent interfaces with increasing and decreasing impedance with depth, respectively. Horizontal distances are referenced to the surface trace of the MFT. All depths are relative to sea level. S represents the Siwaliks, LH the Lesser Himalaya and HH the Higher Himalaya. (B) Initial model geometry proposed from geophysical data with major structures and kinematic partitioning shown by colored arrows. The crustal ramp is inferred from the microseismic data of Pandey et al. (1999). V_o and V_u are the total overthrusting and underthrusting velocities, respectively; the former is partitioned between overthrusting taken up by the MFT (V_{mft}) and the out-of-sequence thrust (V_{tf}). For the model shown, $V_{tf} = 6 \text{ km/Myr}$ (light green arrows), $V_{mft} = 0$ and $V_u = 15 \text{ km/Myr}$ (blue arrows).

Modified from Robert et al. (2011).

6.3.2. Effect of out-of-sequence thrusting on thermochronological age patterns

Fig. 16 shows predicted AHe, AFT, ZHe and ZFT ages for a simple overthrusting model (no out-of-sequence thrusting along the MCT), as well as models including Quaternary out-of-sequence thrusting at different velocities. In these latter models, overthrusting takes place along the MHT only for the first 8 Myr of the model run (10 to 2 Ma). For the last 2 Myr (2 Ma to today) the overthrusting is partitioned between the MHT and the MCT, to simulate Quaternary reactivation of the MCT (as suggested by Hedges et al., 2004). The velocity along the MCT during the out-of-sequence thrusting event (V_{tf}) is set to different values between 0 and 6 km/Myr. The thrusting velocity along the MFT is diminished accordingly so that the total overthrusting velocity remains constant at 6 km/Myr.

Out-of-sequence thrusting has two main effects on the age pattern. First, as expected, AHe, AFT and ZHe ages in the Lesser Himalaya (south of the MCT) become older with increasing activity of the out-of-sequence thrust and consequent decrease of velocity on the MHT; for $V_{tf} \geq 4 \text{ km/Myr}$, none of the thermochronological systems is reset in the southern part of the Lesser Himalaya. However, except for these extreme models where nearly all overthrusting is taken up on the out-of-sequence thrust, the models do not predict a clear age jump across the topographic transition zone (where the MCT intercepts the surface). This is because, in these models, out-of-sequence thrusting

has not been going on for long enough to influence the AFT ages in the Higher Himalaya.

Secondly, the width of the reset age window above the MHT crustal ramp increases with increasing out-of-sequence velocity. Surprisingly, models corresponding to the highest overthrusting velocities also predict older ages within the hanging wall of the out-of-sequence thrust. This is because the hanging wall of the out-of-sequence thrust is much thinner in the MCT zone than elsewhere along the MHT, so that the thermal perturbation associated with overthrusting is much smaller, and the near-surface thermal gradient consequently lower, when a significant proportion of the overthrusting velocity is taken up by the out-of-sequence thrust.

Finally, it is worth noting that the effect of a fault on the distribution of surface ages is also strongly influenced by the closure temperature of the thermochronological system. Even in cases where convergence rates are important, higher-temperature systems (ZHe, ZFT) appear much less sensitive than lower-temperature systems (AHe, AFT; Fig. 16) to variations in convergence velocity as imposed here by varying the component of out-of-sequence thrusting.

We can now compare the observed AFT age dataset (for locations where AFT samples were collected) with predicted AFT ages for the two end-member model runs, i.e., $V_{tf} = 0$ and $V_{tf} = 6 \text{ km/Myr}$ (Fig. 17). None of the models assuming out-of-sequence faulting fits the observed Lesser Himalayan ages (at latitudes $< 28^\circ \text{ N}$); all out-of-

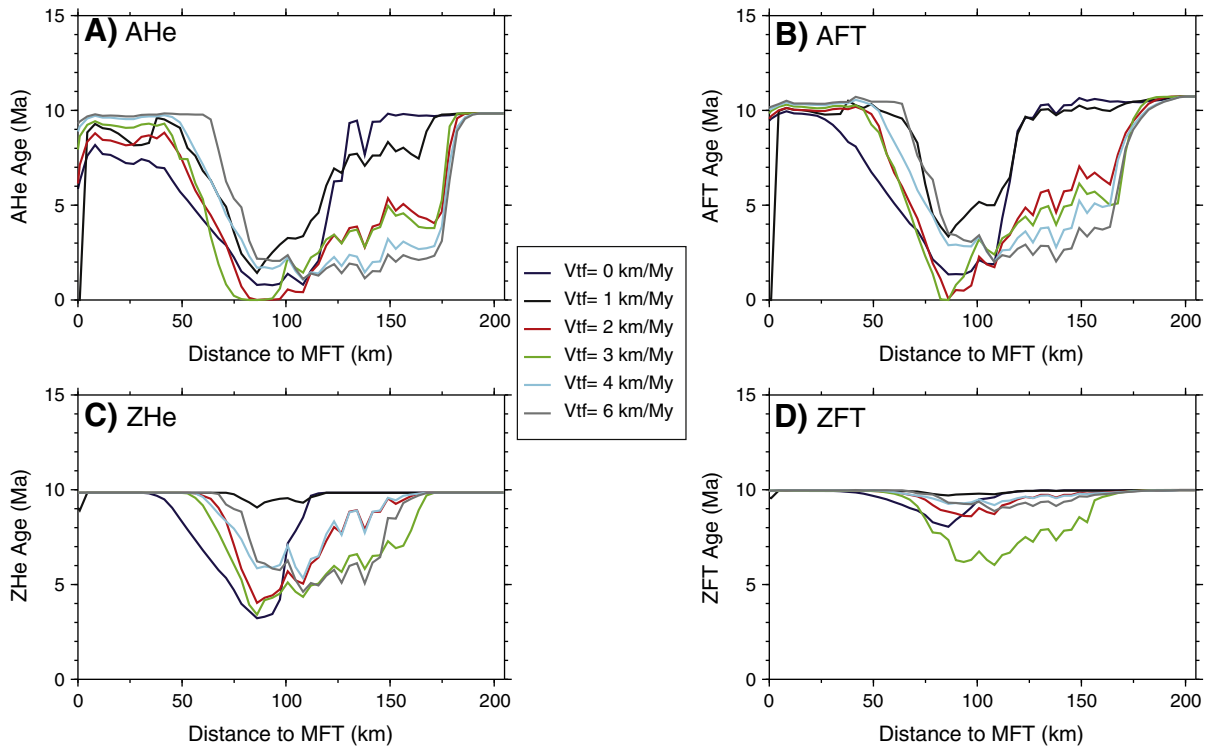


Fig. 16. Predicted apatite (U-Th)/He (AHe; A), apatite fission-track (AFT; B), zircon (U-Th)/He (ZHe; C) and zircon fission-track (ZFT; D) age patterns for the model shown in Fig. 15 as a function of Quaternary out-of-sequence thrusting velocity on the MCT (V_{tf}); the overthrusting velocity on the MHT is equal to $6 - V_{tf}$ km/Myr in these models.

thrusting scenarios also predict a sharper transition toward young ages than is observed across the MCT and topographic transition zone. However, the very young ages (~ 1 Ma) predicted above the MHT crustal ramp in the High Himalaya (north of latitudes $< 28^\circ$ N) fit well the observed AFT ages. In contrast, models without out-of-sequence faulting fit the observed northward decreasing age-trend across the Lesser Himalaya relatively well, but predicted ages increase northward of the MCT in contrast to constant observed AFT ages in the Higher Himalaya. We conclude that although the existing age dataset cannot easily constrain the recent activity of the MCT, it does not apparently require out-of-sequence thrusting on the MCT (Robert et al., 2009). A full exploration of the kinematic history has been performed using inversion techniques as described in the previous section in two recent studies (Herman et al., 2010a; Robert et al., 2011), both concluding that the most reasonable fit to the data is obtained for models in which all motion is taken up by the MHT (i.e., without out-of-sequence thrusting).

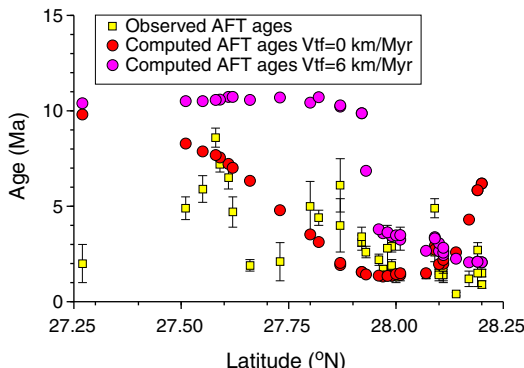


Fig. 17. Comparison of observed and predicted AFT age patterns for the central Nepal Himalaya transect as a function of out-of-sequence thrusting velocity (V_{tf}); the overthrusting velocity on the MHT is equal to $(6 V_{tf})$ km/Myr in these models.

7. Detrital thermochronology

7.1. Motivation

Detrital thermochronology records the cooling history of samples collected from the sediments shed off eroding mountain belts, as opposed to classical “in-situ” thermochronology that focuses on rocks outcropping in the mountain belt today. The use of this method for analysis of ancient and modern sediments has proven a powerful tool for predicting the sedimentary provenance, exhumation histories, past erosion rates and patterns of orogens (Garver et al., 1999; Bernet and Spiegel, 2004). The major advantage of this method as compared to classical, in-situ sample analysis is that the evolution of exhumation and cooling rates through time can be monitored using samples of variable depositional ages (e.g., Bernet et al., 2006, 2009). Age data from orogenic material contained in the sedimentary basins surrounding mountain belts contains a much longer-term record of the evolution of their source areas than present day in-situ ages, in particular for rapidly exhuming active mountain belts. They also contain a synoptic view of erosion within the source area, which can in principle be inverted for the spatial distribution of erosion within the source area, if the in-situ age-structure is known (e.g., Brewer et al., 2003; Ruhl and Hodges, 2005; Vermeesch, 2007; Avdeev et al., 2011; Tranel et al., 2011). However, direct inference of source-area exhumation from detrital thermochronology data is even more difficult than for in-situ data (Rahl et al., 2007; Whipp et al., 2009). It is for these reasons that the new version of PECUBE includes a new module for the prediction of detrital age distributions.

7.2. Generation of predicted detrital age distributions

To simulate detrital age distributions, PECUBE produces surface-age distributions at set times in the past. These are obtained by computing the thermal histories of rock particles that end up at the surface of the model at these times, in an identical manner as for

the points that end up at the surface at the end of the model run. These additional calculations do not significantly increase the model run time as the computation time for rock-particle tracking and thermochronological age prediction is relatively minor compared to the computational cost of solving the large three-dimensional thermal problem.

The thermal histories of rock particles that are at the surface at set times during the model run are obtained in two steps. First, rock particles are placed at the surface of the model at the required set times, and using the imposed tectonic and relief change scenarios, their original position is back-calculated. Secondly, during the forward temperature calculations, the points are progressively advected toward their final position and their temperature history is recorded. At each of the set times, the cooling ages are calculated from the $T-t$ paths. Several thermochronometers can be simulated using the techniques outlined in Section 3.

7.3. Comparing PECUBE predictions to observed detrital distributions

Cooling-age distributions of a detrital sample may be effectively described in terms of a synoptic probability density function (SPDF; Brewer et al., 2003; Ruhl and Hodges, 2005). For each grain dated by a given thermochronological system, the measured age, t_c , and the uncertainty in the age (standard deviation), σ_{t_c} , define a probability density function (PDF) of age, t . Following Ruhl and Hodges (2005), we assume a normal distribution of error. In this case, the calculated probability density function (PDF_c) of age for each measured single-grain age (t_c) is given by:

$$PDF_c = \frac{1}{\sqrt{2\pi}\sigma_{t_c}} \exp\left[-\frac{1}{2}\left(\frac{t-t_c}{\sigma_{t_c}}\right)^2\right] \quad (19)$$

where σ_{t_c} is the calculated one-sigma age uncertainty and t is the range of ages over which PDF_c is defined. We can combine all n_c single-grain age measurements in a sample to define a SPDF of ages:

$$SPDF_c = \frac{1}{n_c} \sum_{i=1}^{n_c} PDF_c(i). \quad (20)$$

Note that the SPDF is normalized by dividing by the number of single-grain ages in the sample.

We can similarly define a PDF of predicted ages from the collection of ages calculated for points at the surface at a given time in the model (or part of it). The model probability density function (PDF_m) is:

$$PDF_m = \frac{1}{\sqrt{2\pi}\sigma_{sys}} \exp\left[-\frac{1}{2}\left(\frac{t-t_m}{\sigma_{sys}}\right)^2\right] \times \frac{\dot{\varepsilon}}{\dot{\varepsilon}}. \quad (21)$$

To do this, a synthetic sample uncertainty σ_{sys} must be assigned to each predicted thermochronological age. In the following, we assume $\sigma_{sys} = 10\%$ for ZFT and 2% for MAR (Argon in Muscovite ages), representing typical errors associated with grain-age reproducibility and analytical uncertainties in these two systems. t is the range of ages over which PDF_m is defined. We choose to scale the magnitude of PDF_m age peaks by the corresponding exhumation rate normalized by the mean model exhumation rate ($\frac{\dot{\varepsilon}}{\dot{\varepsilon}}$), similar to the method of Whipp et al. (2009), in order to account for the expectation that regions with higher exhumation/erosion rates will provide a correspondingly larger quantity of datable grains to the sediment sample.

Finally, the age distribution of the entire model space is determined by summing the individual age PDF_m s, giving the model synoptic probability function ($SPDF_m$),

$$SPDF_m = \frac{1}{n_m} \sum_{i=1}^{n_m} PDF_m(i) \quad (22)$$

where n_m is the number of predicted ages in the model space, and the predicted $SPDF_m$ is normalized similarly to the observed $SPDF_c$ to allow comparison of observed and predicted ages.

Predicted and measured age distributions are compared using the probability density and cumulative probability density functions for each of the predicted and measured age distributions. Cumulative density functions allow easy comparison in terms of misfit between the predicted and measured grain age distributions. We use the cumulative synoptic density functions (CSPDFs) which represent the probability that the age takes on a value less than or equal to t :

$$CSPDF_{c,m} = \sum_{j=0}^t SPDF_{c,m}(j). \quad (23)$$

In order to quantitatively compare predicted and observed grain-age distributions, we use the Kolmogorov–Smirnov statistic (KS-test; Vetterling et al., 1992), which is simply the maximum value of the absolute difference between two cumulative distribution functions. The misfit defined in this way provides the basis for inversion analysis to determine the optimal tectonic and erosional scenarios as discussed in Section 4.

It has been argued (Ruhl and Hodges, 2005, e.g.) that the Kuiper statistics provides a more discriminant test for comparing observed and predicted detrital age distributions. As the Kuiper statistics is relatively similar to the K-S statistics (Vetterling et al., 1992), we plan on implementing both into PECUBE in the very near future. In the current version, PECUBE only produces age distributions and it is left to the user to compare them to observed distributions, if required.

7.4. Case study: Analyzing the detrital thermochronology record in the Siwaliks of Nepal

To illustrate our approach and show how PECUBE can be used to extract tectonic/geomorphic information from detrital datasets, we have used two low-temperature detrital datasets collected along the same stratigraphic sections within the Miocene to Pliocene Siwalik Group (Nepal), and from modern rivers in western and central Nepal. The Siwalik Group is formed by detrital deposits (mainly fine- to coarse-grained sandstones and conglomerates) of the Himalayan foreland basin that have been incorporated into the orogenic belt and, as a consequence, uplifted, eroded and deformed during the last few Myr (e.g., DeCelles et al., 2001; Mugnier et al., 2004). These deposits contain a continuous record of Himalayan erosion since at least ~15 Ma, the onset age of deposition of the Siwalik Group (Gautam and Fujiwara, 2000; Ojha et al., 2009). The first data set consists of detrital zircon fission-track ages from Siwalik sandstone and modern river-sand samples (Bernet et al., 2006), while the second dataset contains $^{40}\text{Ar}/^{39}\text{Ar}$ ages of detrital white micas collected along the same stratigraphic sections (Szulc et al., 2006). Samples from these two datasets have depositional ages between ~15 Ma and present-day, therefore allowing for a rather comprehensive assessment of Miocene–Pliocene regional exhumation rates in the central Himalaya.

To interpret the datasets, age distributions for the two thermochronological systems (ZFT and MAR) are predicted at times, t_s , that correspond to the stratigraphic ages of the detrital age samples, using PECUBE and the geometry and kinematics previously established for the central Himalaya (Robert et al., 2009, 2011, cf. Section 6). As an example of the use of this type of analysis, we show in Fig. 18 a typical comparison between grain-age distributions (for a single stratigraphic age), in terms of the corresponding PDF and CSPDF. In the example shown, we have used the detrital age data to constrain the age of motion on the main thrust faults along the Himalayan front. The best-fitting scenario in this case corresponds to a simple southward (in-sequence) propagation of deformation. The detrital data provides direct constraints on the timing and duration of motion on each

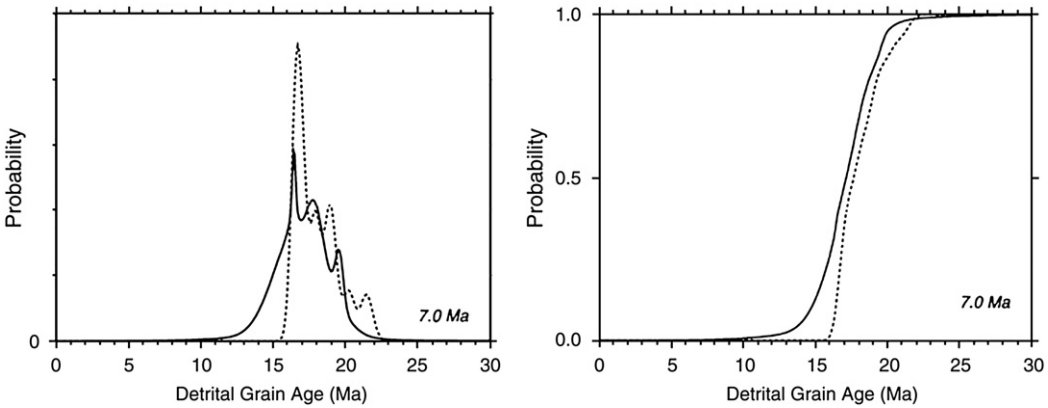


Fig. 18. Measured (solid lines) and predicted (dotted lines) white-mica $^{40}\text{Ar}/^{39}\text{Ar}$ (MAR) grain-age distributions represented in terms of a synoptic probability density function (SPDF; left panel) and the cumulative synoptic density function (CSPDF, right panel). The model grain-age distributions were obtained by running the model from 25 Myr to present. The measured dataset is from Szulc et al. (2006). These measured and predicted age distributions correspond to a stratigraphic age of 7 Ma. The modeled region simulates structures in central Nepal Himalaya including the northward dipping Main Frontal (MFT), Main Boundary (MBT), “intermediate” and Main Central (MCT) thrusts active from ~20 Ma to present-day. Fault activity is assumed to propagate southward through time.

structure. Although the result shown in Fig. 18 corresponds to a forward-model run, detrital datasets can be inverted in exactly the same manner as in-situ data in order to explore the parameter space and place constraints on model parameter values (in this case, timing and rate of motion along faults), using the KS probabilities that the measured and predicted age CSPDFs are similar as objective functions.

8. Linking PECUBE to a landscape-evolution model

8.1. Motivation

Landscape evolution results from the balance between a variety of surface processes and vertical motions caused by tectonic forces. The relative importance of the various surface processes remains difficult to assess, and in particular determining the relative efficiency of fluvial and glacial processes since the onset of Quaternary periodic glaciations has proved to be a complex question (e.g., Whipple et al., 1999; Brocklehurst and Whipple, 2006; Naylor and Gabet, 2007; Egholm et al., 2009). Furthermore, feedbacks must exist between surface processes and the underlying tectonics (e.g., Whipple, 2009, and references therein), but the strength of these feedbacks remains ultimately linked to the response time of one forcing mechanism to changes in the other.

Landscape-evolution (or surface-process) models (SPM) aim to capture the main controls on landscape development over geological times from mathematical description and spatio-temporal “upscale” of physical processes operating at small spatial and temporal scales. As such, they represent a more or less sophisticated, yet inherently approximate representation of the different processes working at the Earth's surface. Therefore, when constructing and using a SPM, one needs to assess whether the predictions in fact represent the simulated landforms. Furthermore it is desirable also to constrain the rates at which the landforms are created, and how the surface processes respond to external forcing (such as a change in climatic or tectonic conditions). It has been argued (e.g. van der Beek and Braun, 1998) that the predicted rates of landscape change may in fact be more discriminatory to assess the performance of SPMs than the predicted final form of the landscape on geological timescales. The advantages of combining SPMs with PECUBE to obtain constraints from low-temperature thermochronological data are therefore twofold:

1. to constrain the validity of a SPM by direct comparison with observations. In this regard PECUBE can also be used to predict the adequacy of potential sampling strategies in resolving particularly important aspects of the evolution of the landscape (e.g. where to sample, which thermochronometers to use).

2. to discriminate between competing processes and/or quantify their respective contribution to the formation of the observed landscape.

Although all of the above examples have used simplified parametric descriptions of landscape change (i.e. Sections 4 and 5), we have devoted much work over recent years to allow PECUBE to predict thermochronological ages directly from the results of various SPMs, in the hope of providing quantitative means to constrain the efficiency of and discriminate between competing surface processes or underlying tectonic controls (e.g. Braun and van der Beek, 2004; Herman et al., 2010a). This has concerned in particular the coupling of PECUBE to the CASCADE SPM, which simulates fluvial erosion, transport and deposition, and hillslope processes (for a full description of the code, see Braun and Sambridge, 1997). During the course of this work, a module has been added to PECUBE to extract from the CASCADE output files the information necessary to build the required input files to couple it to PECUBE. This module can serve as a template to develop similar modules to couple PECUBE to other landscape-evolution models, and in the example we develop below we couple PECUBE to a new fluvio-glacial SPM, iSOSIA (Egholm et al., 2009, 2011).

8.2. Working procedure

The first version of PECUBE (Braun, 2003) had already been designed to accept any representation of surface topography and its evolution through time, i.e., it is not restricted to simple topographic models constructed on a rectangular grid, and is therefore ideally suited to be combined with any SPM. We have therefore included in PECUBE the possibility to use as input surface topography the results of a SPM in the form of a set of topographic surfaces computed by the SPM.

For computational efficiency and because there is little, if any, potential for feedback between the temperature field predicted by PECUBE and the surface processes, the two models (the SPM and PECUBE) are run sequentially. The SPM is required to produce a set of files containing the position of the nodes at which the topography is predicted at different times; these can be positioned along a regular rectangular grid, in which case the geometry of the grid has to be specified (position of bottom left corner, spacing between and number of mesh points in both directions), or at arbitrarily spaced points, in which case the topology of the triangles connecting the points must also be provided. The files must contain the height of the topography, the rate of vertical rock uplift and the surface temperature. The vertical rock uplift has to be specified to insure that the rock uplift used in the

SPM and PECUBE are identical. The temperature files are useful if the SPM required the computation of the surface temperature, as is the case for SPM including glacial erosion processes. One set of files is required for each time step that is defined in the PECUBE input file. Note that when using PECUBE together with a SPM, vertical rock uplift only is considered, as specified in the uplift file from the SPM. This means that no displacement field including movement along faults and/or isostatic compensation should be used at present in PECUBE. Some SPMs, in particular CASCADE, include the isostatic response to surface erosion in their output.

Although the incorporation of a more detailed topographic evolution, as predicted by a SPM, will lead to higher computational costs in PECUBE, the highest cost will undoubtedly be related to the SPM itself. It is therefore not recommended to use PECUBE in inversion mode when using it in combination with a SPM.

8.3. Example: Combining PECUBE with a fluvio-glacial SPM

To illustrate how PECUBE can be combined with a SPM, we show here predicted AHe ages derived from a fluvio-glacial surface-process model (iSOSIA) coupled to PECUBE. iSOSIA contains a computationally efficient yet high-order ice-sheet model coupled with fluvial erosion and hillslope mass wasting (Egholm et al., 2009; Egholm et al., 2011). We investigate how spatial patterns in AHe ages are affected when transforming a fluvial steady-state landscape into a transient glacially-affected landscape.

Through its higher-order ice dynamics, iSOSIA takes into account effects that are not present in standard “shallow-ice” simulations (e.g. Braun et al., 1999). These effects arise from steep bed topography and the resulting large spatial gradients in ice thickness, flow velocity, and horizontal stress, which are all important when simulating ice flow in Alpine settings (Egholm et al., 2011). Constants related to deformation and sliding are tuned so that ice-sliding velocities do not exceed realistic values, i.e. 0–100 m/yr. Glacial erosion is proportional to sliding velocity (e.g. Hallett, 1979, 1996), with a proportionality constant that is not well known but scaled to first order by the prediction of realistic glacial landscapes (deep U-shaped valleys, hanging valleys, cirques, steep head walls etc.; Egholm et al., 2009). Parameters controlling the efficiency of fluvial and hillslope processes define the fluvial landscape, and are selected such that the initial landscape is in steady-state with the imposed tectonic rock uplift and results in a finite-amplitude “reasonable” relief. Calculations are done on an irregularly discretized 40 km × 80 km rectangular grid, with a 40-km thick crust below for the thermal calculations. The average grid resolution at the surface is approximately 815 m. In the vertical direction, the resolution increases toward the surface with an average node spacing of approximately 1000 m. The temperature is fixed at 800 °C at the base of the crust, thermal diffusivity is set to 25 km²/Myr, and heat production is neglected. AHe ages are computed following the procedure and parameter values described in Section 3.2.

We generate the initial fluvial steady-state landscape from a nearly flat surface by introducing a uniform tectonic rock-uplift rate of 0.07 km/Myr. Due to flexural isostatic compensation of the unloading caused by erosion, the total rock-uplift rate is higher, reaching approximately 0.5 km/Myr at fluvial steady-state (NB, note that in iSOSIA isostatic rebound is calculated in response to the total erosion at any time, in contrast to CASCADE and PECUBE, which predict isostatic response to changing surface topography only). Initially only fluvial and hill-slope erosion processes are active, by fixing the model snowline at 3000 m, i.e. above the maximum topography. In the steady-state fluvial landscape (Fig. 19A,B), predicted AHe ages follow a simple age-elevation relationship; the age predictions, represented by colors on Fig. 20A, are found to correlate well with the topographic contours. This close to linear relationship between age and elevation is also apparent when plotting age vs. elevation at fluvial steady-state for all cells in the model (Fig. 21A). Ages range from approximately 3.5 Ma at

low elevations up to nearly 7 Ma at the highest elevations. After reaching geomorphic and thermal steady-state, we ran the model through three 100-kyr glacial cycles, which we represented by a periodic variation in snowline altitude between 1800 m and 2575 m (Fig. 19G, black). Fig. 19C–K shows, for selected times in the first of these cycles, the extent of glaciation in the landscape and the cumulative glacial erosion (snapshots indicated in Fig. 19G by black lines). Total glacial erosion is at its maximum in the first cycle, up to nearly 700 m on average in 100 kyr Fig. 19K. In the following two cycles, the glacial erosion rate decreases, due to decreasing mean topography and relief (orange and green curves in Fig. 19G). The lowering of mean topography minimizes the area available for snow and ice accumulation, leading to a decreasing glacial extent, as evidenced in Fig. 19G (blue curve), and, consequently, lower glacial erosion rates. Some areas experience erosion rates of up to 12 km/Myr in the first cycle, whereas the average erosion within the entire period is at most 4.7 km/Myr. As flexural isostatic rebound is calculated from total erosion, the higher erosion rates through the glacial cycles will lead to an increase in total rock-uplift rate, in average approximately 1.5 km/Myr, affecting also areas that are not experiencing glacial erosion. The final glacial landscape (Fig. 19L, M) shows characteristic glacial morphologies including deep U-shaped valleys, hanging valley, cirques, and steep headwalls, suggesting that glacial landscape formation can be predicted and thus explained by the ice dynamics of the iSOSIA model (Egholm et al., 2011).

Glacial erosion leads to a more complex age-elevation relationship (Fig. 20B–F), as the AHe ages do not seem to follow closely the contours in the landscape. The pattern is evident especially in the main valleys, as can be seen in detail on Fig. 20E, but can also be seen on the main ridges. This more complex age-elevation relationship is apparent also when comparing the age-elevation trend from all cells in the glacial landscapes with the same trend for the initial fluvial landscape (Fig. 21); the trend is not only broader, but the youngest ages seem not to occur at the lowest elevations but some 700–1000 m further up in the landscape. The AHe ages thus record the particularly efficient glacial cirque erosion at the headwaters of major valleys (Fig. 19H–K).

The spatial patterns in predicted AHe ages imply that glacial erosion in Alpine settings leads to more complex exhumation patterns than erosion by fluvial and hillslope processes, and that periodic cycling through glacial-interglacial climate conditions introduces additional complexity. The AHe-age minimum at intermediate elevations suggests focusing of glacial erosion in large valleys and cirques as observed in mountainous regions affected by Quaternary glaciations (Shuster et al., 2011; Valla et al., 2012). These preliminary results demonstrate the potential of coupling PECUBE and SPMs to constrain the efficiency of various surface processes and the adequacy of the models we have built to represent them.

9. Future improvements

The PECUBE code is under continuous development, as potential improvements are suggested or potential problems recognized by ourselves or others in the thermochronological community. To round up this synthesis, we will briefly discuss below some of the major improvements we expect to introduce to the code in the near future.

9.1. More detailed thermal structure

The current default in PECUBE is to impose uniform thermal properties (i.e., heat production, thermal conductivity, basal temperature) throughout the modeling domain. It has been realized for several years that this setup may lead to an unrealistic temperature structure in the lower part of the model domain, but as long as the main use of PECUBE was to predict the effects of transient topography on low-temperature thermochronometers (e.g. Sections 4, 5, and 8) this was

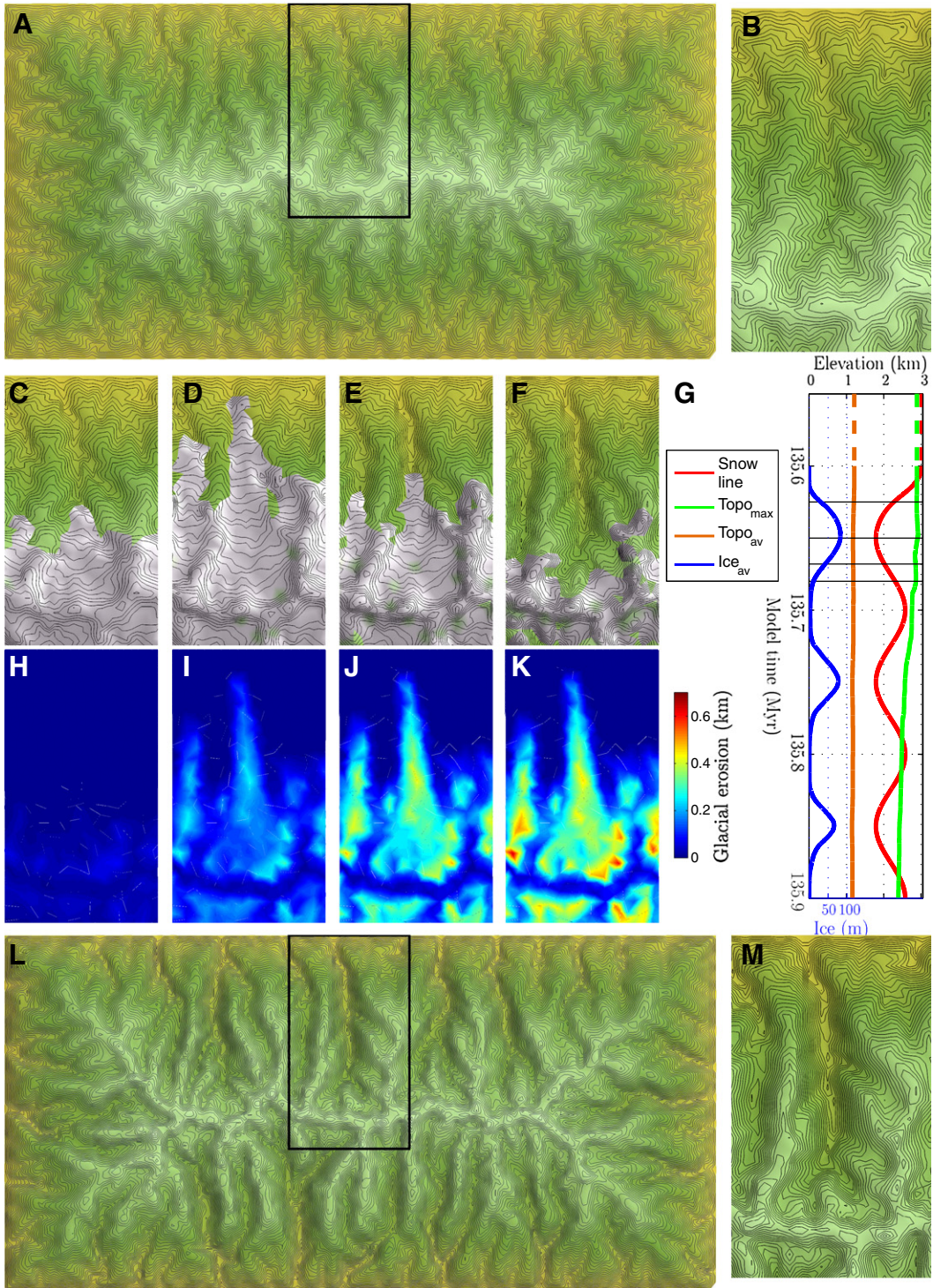


Fig. 19. Model results showing the evolution of a fluvial steady-state landscape into a glacially-influenced landscape by introducing an oscillating climate (100-kyr period glaciations). (A) Initial steady-state fluvial landscape, after running the SPM for 135 Myr. The boxed catchment is enlarged in (B). (C–F) Snapshots of glacial extent on the evolving topography during the first glacial cycle. The timing of the snapshots is indicated with black lines in G. (G) Evolution of the snowline (red), maximum topography (green), mean topography (orange), and average amount of ice in the landscape (blue) with model time since the formation of a fluvial steady-state landscape at 135 Myr. Black lines indicate the timing of snapshots shown in (C–K) during the first glacial cycle. (H–K) Snapshots of accumulated glacial erosion within the first glacial cycle. Total glacial erosion within the first glacial cycle is nearly 700 m for some areas. (L) Final glacial landscape. The boxed catchment is enlarged in (M) and shows characteristic glacial morphology including a deep U-shaped valley, a hanging valley, cirques, and steep headwalls.

not considered a serious issue. However, the recent use of PECUBE to study more “tectonic” problems (e.g. Sections 6 and 7) and the consequent implementation of higher-temperature systems (in particular $^{40}\text{Ar}/^{39}\text{Ar}$ on micas and hornblende) does require a consistent prediction of thermal structure throughout the model domain. Implementation of a

heat-production term that exponentially decreases with depth or is limited to a surface layer is relatively straightforward, but requires tracking the thermal properties of rocks in the model (Ehlers and Chapman, 1999). This becomes a more difficult and computationally expensive task to perform accurately, especially in the presence of faults.

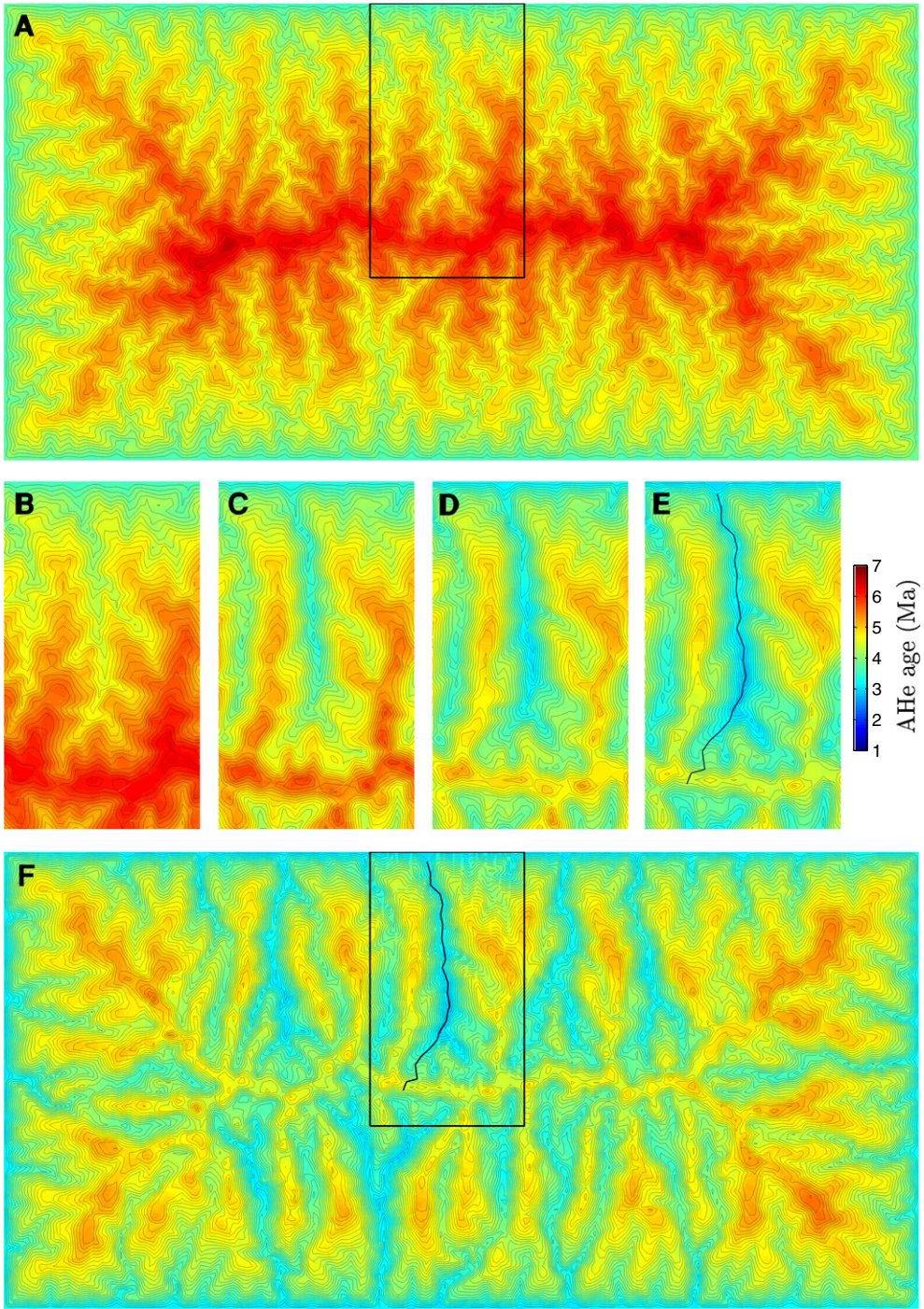


Fig. 20. Predicted evolution of AHe ages for the model results shown in Fig. 19. Ages are represented with color, whereas the contours represent the topography. (A) AHe age predictions for the initial fluvial steady-state landscape. The boxed catchment is enlarged in (B). There seems to be a simple close to linear relationship between age and elevation, as the ages correlate with the topographic contours. (B–E) snapshots of the evolution in AHe ages, from the initial fluvial landscape to the final glacial landscape in (F). The snapshots (C–E) represent the AHe ages found at the surface after each of the three glacial cycles. (F) AHe age predictions in the final glacial landscape show a more complex age-elevation relationship, as younger ages are found higher up in the landscape. The boxed catchment is enlarged in (E). The black line represents the longitudinal profile plotted with error bars in Fig. 21D.

Direct temperature or heat flow measurements could also be included to help constrain the inversion procedure. Alternatively, in models including faults, variable thermal properties can be defined for the blocks delimited by these faults (c.f. Herman et al., 2010a).

Similarly, the thermal effects of “blanketing” by low-conductivity sediments or volcanics (Jeffreys, 1931) that may have once overlain the eroded section, or conversely the “cooling” effect of highly permeable overlying sediments that allow efficient advective heat transport (Bredehoeft and Papadopoulos, 1965), will have significant effects on

spatial and temporal cooling patterns and therefore on thermochronological ages. These effects can also be taken into account by allowing thermal conductivities to vary with depth and advecting the thermal properties with the exhuming rock particles.

Although the study regions modeled with PECUBE will generally be sufficiently restricted and uniform to justify laterally constant thermal parameters, a particular case is constituted by Andean- or Cordilleran-type orogens, which display a significant increase in geothermal gradient when moving from the fore-arc to the magmatic

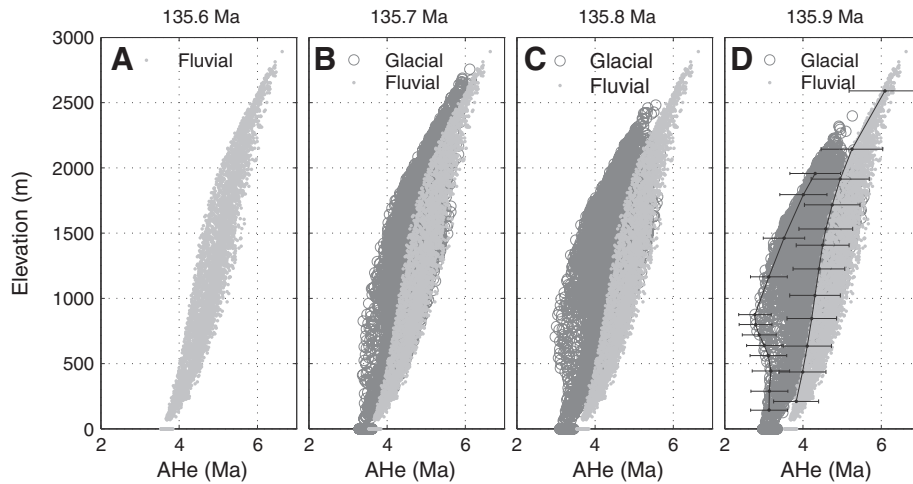


Fig. 21. AHe age-elevation relationships for the landscape at different times (all cells are represented in the plot). (A) Age-elevation relationship for the initial steady-state fluvial landscape. (B–D) represent the relationships after each of the three glacial cycles. The error bars plotted in (D) represent 15% uncertainty for the longitudinal profile marked in Fig. 20E,F.

arc. Modeling such systems in their entirety requires imposing a spatially varying thermal structure, for instance by allowing the basal temperature to vary laterally (Schildgen et al., 2009). A comparable problem is posed by potential temporal variations in thermal structure in Cordilleran-type orogens, due to transient heating associated with magmatic pulses. An attempt has been made to model these by allowing temporal variations in heat production throughout the model domain and it has been shown that including this effect may lead to more internally consistent quantitative interpretation of thermochronological datasets, for instance in the Cascade Mountains of the Northwestern USA (Simon-Labrec, 2010). A physically more realistic approach that specifically models the thermal effect of magmatic intrusions is possible, however, and will be developed in the near future.

Finally, a major unknown remains the effect of topography-driven groundwater flow on the transport of heat in the crust. This potentially important mechanism tends to depress the geothermal gradient in the infiltration areas under high topography and compress it in the valleys, thus counteracting the effect of topography on the conductive thermal structure. Its effects on the distribution and interpretation of thermochronological ages could be significant (Whipp and Ehlers, 2007) and in particular in the case of borehole and/or tunnel data such as those used in the example described in Section 5 (Glotzbach et al., 2008). Widespread occurrence of valley hot springs in active mountain belts (e.g., Shi et al., 1996; Derry et al., 2009) provides support for this mechanism, although the location of springs also appears strongly controlled by major crustal faults. A numerical implementation of advective heat transport through topography-driven groundwater flow has been developed and will be implemented into PECUBE shortly.

9.2. Complex velocity fields

As explained in Section 6, some issues remain concerning either non-conservation of mass or problematic deformation patterns in models simulating simultaneous or subsequent activation of multiple faults. This is because fault-controlled kinematics are implemented in PECUBE in a relatively simplified manner. Structural modeling packages such as 2DMove™ or THRUSTPACK™ are able to handle more complex kinematics, as observed for instance in foreland fold-and-thrust belts, and their effects on thermal structure and thermochronological age patterns have been explored in 2D (Husson and Moretti, 2002; Lock and Willett, 2008). We have recently started working on the option of importing an arbitrary velocity field

obtained from such modeling packages or any other source in PECUBE (Erdos et al., 2011).

9.3. Better coupling with surface-process models

As outlined in Section 8, current coupling of PECUBE and surface-process models that predict landscape evolution through time is restricted to models that include vertical particle paths (rock-uplift) only. However, it is not complicated to extend the coupling to more complex tectonic settings, as the same kinematics can be used to drive landscape evolution and to predict the thermal field and cooling patterns of rocks ending up at the surface (Herman and Braun, 2006; Herman et al., 2007, 2010a). Future developments will include fully flexible coupling between any imposed kinematic field, prediction of landscape response through a surface-process model and prediction of the thermal response and its thermochronological record using PECUBE.

9.4. Advanced age-prediction models

The initial philosophy when designing PECUBE was to predict thermochronological ages at all points representing the surface of the model and then sample/interpolate these to obtain predicted ages at the sample locations to compare with observed ages. Therefore, the age-prediction models implemented were chosen to be relatively simple and represent some average system behavior. However, detailed comparison of predicted and observed thermochronology data requires taking into account secondary (non-thermal) effects that can affect the data. The annealing of fission-tracks is known to be influenced by chemical composition in apatite (e.g. Ketcham et al., 1999, 2007) and radiation damage in zircon (e.g., Tagami et al., 1998). Likewise, recent studies have shown that the retention of He in apatite is also controlled by radiation damage (Flowers et al., 2009; Gautheron et al., 2009). For the K-feldspar $^{40}\text{Ar}/^{39}\text{Ar}$ system, diffusion kinetics appear to depend on the sample-specific distribution of diffusion domains (e.g. Lovera et al., 1991). As the modeled scenarios become more complex, it becomes important to take such effects into account when comparing model predictions with measured data. This requires, however, each sample to be modeled individually.

The incorporation of the Ketcham et al. (1999) AFT annealing model now allows incorporating chemical control on AFT annealing kinetics. We have recently also incorporated an AHe-diffusion model that takes radiation-damage production and annealing into account (Gautheron et al., 2009) in PECUBE Valla et al. (2012).

These developments allow more detailed data-model comparison that take into account sample specifics.

A related development concerns the prediction of thermochronometer characteristics that record the sample cooling path below its closure temperature, such as fission-track length distributions in AFT, $^{40}\text{Ar}/^{39}\text{Ar}$ step-heating data or the recently developed $^4\text{He}/^3\text{He}$ thermochronometer (Shuster and Farley, 2004). Together with implementation of the Ketcham et al. (1999) AFT annealing model, PECUBE now also allows predicting the full AFT length distribution and its comparison to an observed distribution through a Kolmogorov–Smirnov test. For comparison with $^4\text{He}/^3\text{He}$ or $^{40}\text{Ar}/^{39}\text{Ar}$ step-heating data, two approaches are possible: the time–temperature history predicted by PECUBE for a specific sample point can be compared with the history inferred by modeling the data (cf. Schildgen et al., 2010; Valla et al., 2012), or the age-prediction model included in PECUBE could be used to predict synthetic step-heating spectra that can be directly compared to the observed spectra. We anticipate developing modules that would allow taking this second approach. Also, the ability to specify grain size for each individual sample is an obvious improvement that should soon be included in PECUBE.

Finally, as the new very-low-temperature OSL thermochronometer (Herman et al., 2010b) becomes better understood and more widely developed and used, we will develop the necessary modules to predict this type of data from PECUBE scenarios.

10. Conclusion and code availability

Since its inception nearly a decade ago, the PECUBE code has been continuously amended and improved. These modifications to the code have been motivated by new questions that we were trying to address or interpretational dilemmas that we were facing, as well as by specific requests from others within the thermochronological community. This contribution has aimed to provide a synthesis of the current state of development of the model. It is definitely not a description of a status-quo, however, as new modifications to and developments of the code are continuously being made. In the last decade, numerous thermochronologists, tectonicists or geomorphologists have used PECUBE to address their specific problems, and in nearly all cases at least some minor modification has proven necessary. It is our hope and anticipation that this healthy development of the code will continue over the years to come.

The code is available by download from the subversion server at ETH: <http://svn-geo.ethz.ch/> after registering with that server. Future improvements to the code will also be made available through this server. Alternatively, the code can be obtained from its main author, Jean Braun, upon a simple email request. We are maintaining a mailing list to inform all registered users on developments and improvements in the code.

Appendix A. Supplementary data

Supplementary data to this article can be found online at doi:[10.1016/j.tecto.2011.12.035](https://doi.org/10.1016/j.tecto.2011.12.035).

References

- Adams, C., 1981. Uplift rates and thermal structure in the Alpine fault zone and Alpine schists, Southern Alps, New Zealand. In: McClay, K.R., Price, N.J. (Eds.), Thrust and Nappe Tectonics: Geological Society of London, 9, pp. 211–222. Special Publication.
- Akaike, H., 1974. A new look at the statistical identification model. IEEE Transactions on Automatic Control 19, 716–723.
- Avdeev, B., Niemi, N., Clark, M., 2011. Doing more with less: Bayesian estimation of erosion models with detrital thermochronometric data. Earth and Planetary Science Letters 305 (3–4), 385–395.
- Avouac, J.-P., 2003. Mountain building, erosion and the seismic cycle in the Nepal Himalaya. Advances in Geophysics 46, 1–79.
- Batt, G., Brandon, M., 2002. Lateral thinking: 2-D interpretation of thermochronology in convergent orogenic settings. Tectonophysics 394, 185–201.
- Batt, G., Braun, J., 1997. On the thermomechanical evolution of compressional orogens. Geophysical Journal International 128, 364–382.
- Batt, G., Braun, J., Kohn, B.P., McDougall, I., 2000. Thermochronological analysis of the dynamics of the Southern Alps, New Zealand. Geological Society of America Bulletin 112, 250–266.
- Bermúdez, M., van der Beek, P., Bernet, M., 2011. Asynchronous Miocene–Pliocene exhumation of the central Venezuelan Andes. Geology 39 (2), 139–142.
- Bernet, M., Spiegel, C., 2004. Detrital Thermochronology – Provenance Analysis, Exhumation and Landscape Evolution of Mountain Belts, volume 378. Geological Society of America Special Paper, Boulder, Colorado.
- Bernet, M., van der Beek, P., Pik, R., Huyghe, P., Mugnier, J.L., Huyghe, P., Szulc, A., 2006. Miocene to recent exhumation of the central Himalaya determined from combined detrital zircon fission-track and U/Pb analysis of Siwalik sediments, western Nepal. Basin Research 18, 393–412.
- Bernet, M., Brandon, M., Garver, J., Balestrieri, M., Ventura, B., Zattin, M., 2009. Exhuming the Alps through time: clues from detrital zircon fission-track ages. Basin Research 21 (6), 781–798.
- Bollinger, L., Avouac, J., Beyssac, O., Catlos, E., Harrison, T., Grove, M., Goffé, B., Sapkota, S., 2004. Thermal structure and exhumation history of the Lesser Himalaya in central Nepal. Tectonics 23 (5), TC5015. doi: [10.1029/2003TC001564](https://doi.org/10.1029/2003TC001564).
- Bollinger, L., Henry, P., Avouac, J., 2006. Mountain building in the Nepal Himalaya: thermal and kinematic model. Earth and Planetary Science Letters 244 (1–2), 58–71.
- Braun, J., 2002a. Estimating exhumation rate and relief evolution by spectral analysis of age-elevation datasets. Terra Nova 14, 210–214.
- Braun, J., 2002b. Quantifying the effect of recent relief changes on age-elevation relationships. Earth and Planetary Science Letters 200, 331–343.
- Braun, J., 2003. Pecube: a new finite element code to solve the heat transport equation in three dimensions in the Earth's crust including the effects of a time-varying, finite amplitude surface topography. Computational Geosciences 29, 787–794.
- Braun, J., Robert, X., 2005. Constraints on the rate of post-orogenic erosional decay from thermochronological data: example from the Dabie Shan, China. Earth Surface Processes and Landforms 30, 1203–1225.
- Braun, J., Sambridge, M., 1997. Modelling landscape evolution on geological time scales: a new method based on irregular spatial discretization. Basin Research 9, 27–52.
- Braun, J., van der Beek, P., 2004. Evolution of passive margin escarpments: what can we learn from low-temperature thermochronology? Journal of Geophysical Research 109, F04009. doi: [10.1029/2004JF000147](https://doi.org/10.1029/2004JF000147).
- Braun, J., Batt, G., Scott, D., McQueen, H., A.R., B., 1994. A simple kinematic model for crustal deformation along two- and three-dimensional listric normal faults derived from scaled laboratory experiments. Journal of Structural Geology 16, 1477–1490.
- Braun, J., Zwartz, D., Tomkin, J., 1999. A new surface processes model combining glacial and fluvial erosion. Annals of Glaciology 28, 282–290.
- Braun, J., van der Beek, P., Batt, G., 2006. Quantitative Thermochronology. Cambridge University Press.
- Bredehoeft, J.D., Papadopoulos, I.S., 1965. Rates of vertical groundwater movement estimated from the Earth's thermal profile. Water Resources Research 1:325328.
- Brewer, I., Burbank, D., 2006. Thermal and kinematic modeling of bedrock and detrital cooling ages in the central Himalaya. Journal of Geophysical Research 111 (B09409). doi: [10.1029/2004JB003304](https://doi.org/10.1029/2004JB003304) B09409.
- Brewer, I., Burbank, D., Hodges, K., 2003. Modelling detrital cooling-age populations: insights from two Himalayan catchments. Basin Research 15, 305–320.
- Brocklehurst, S.H., Whipple, K.X., 2006. Assessing the relative efficiency of fluvial and glacial erosion through simulation of fluvial landscapes. Geomorphology 75 (3–4), 283–299.
- Brown, R., Summerfield, M., Gleadow, A., 1994. Apatite fission track analysis: its potential for the estimation of denudation rates and implications for models of long-term landscape development. In: Kirby, M. (Ed.), Process Models and Theoretical Geomorphology. John Wiley and Sons Ltd, New York, pp. 23–53.
- Campani, M., Herman, F., Mancktelow, N., 2010. Two- and three-dimensional thermal modeling of a low-angle detachment: exhumation history of the Simplon Fault Zone, central Alps. Journal of Geophysical Research 115 (B10420). doi: [10.1029/2009JB007036](https://doi.org/10.1029/2009JB007036).
- Cattin, E., Avouac, J.-P., 2000. Modeling mountain building and the seismic cycle in the Himalaya of Nepal. Journal of Geophysical Research 105, 13,389–13,408.
- Crowley, K., Cameron, M., Schaefer, R., 1991. Experimental studies of annealing of etched fission tracks in fluorapatite. Geochimica et Cosmochimica Acta 89, 1449–1465.
- DeCelles, P., Robinson, D., Quade, J., Ojha, T., Garzione, C., Copeland, P., Upreti, B., 2001. Stratigraphy, structure, and tectonic evolution of the Himalayan fold-thrust belt in western Nepal. Tectonics 20 (4), 487–509.
- Derry, L.A., Evans, M.J., France-Lanord, C., Darling, R.S., 2009. Hydrothermal heat flow near the Main Central Thrust, Nepal. Earth and Planetary Science Letters 286, 101–109.
- Egholm, D., Nielsen, S., Pedersen, V., Lesemann, J.-E., 2009. Glacial effects limiting mountain height. Nature 460, 884–887.
- Egholm, D., Knudsen, M., Clark, C., Lesemann, J., 2011. Modeling the flow of glaciers in steep terrains: the integrated Second-Order Shallow Ice Approximation (iSOSIA). Journal of Geophysical Research. doi: [10.1029/2010JF001900](https://doi.org/10.1029/2010JF001900).
- Ehlers, T., Chapman, D., 1999. Normal fault thermal regimes: conductive and hydrothermal heat transfer surrounding the Wasatch fault, Utah. Tectonophysics 312, 217–234.
- Ehlers, T., Farley, K., 2003. Apatite (U-Th)/He thermochronometry: methods and applications to problems in tectonic and surface processes. Earth and Planetary Science Letters 206, 1–14.
- Ehlers, T., Armstrong, P., Chapman, D., 2001. Normal fault thermal regimes and the interpretation of low-temperature thermochronometers. Physics of the Earth and Planetary Interiors 126, 179–194.

- Ehlers, T., Willett, S., Armstrong, P., Chapman, D., 2003. Exhumation of the Central Wasatch Mountains: 2. Thermo-kinematic models of exhumation, erosion and low-temperature thermochronometer interpretation. *Journal of Geophysical Research* 108, 2173. doi:[10.1029/2001JB001723](https://doi.org/10.1029/2001JB001723).
- Ehlers, T., Farley, K., Rusmore, M., Woodsworth, G., 2006. Apatite (U-Th)/He signal of large-magnitude accelerated glacial erosion, southwest British Columbia. *Geology* 34, 765–768.
- England, P., Molnar, P., 1990. Surface uplift, uplift of rocks and exhumation of rocks. *Geology* 18, 1173–1177.
- Erdos, Z., Huismans, R., van der Beek, P., 2011. Evaluating balanced section restoration with thermochronological data. *EGU General Assembly Abstract*.
- Farley, K., 2000. Helium diffusion from apatite: general behavior as illustrated by Durango fluorapatite. *Journal of Geophysical Research* 105, 2903–2914.
- Fitzgerald, P., Sorkhabi, R., Redfield, T., Stump, E., 1995. Uplift and denudation of the central Alaska Range: a case study in the use of apatite fission track thermochronology to determine absolute uplift parameters. *Journal of Geophysical Research* 100, 20175–20191.
- Fitzgerald, P., Muñoz, J., Coney, P., Baldwin, S., 1999. Asymmetric exhumation across the Pyrenean orogen: implications for the tectonic evolution of a collisional orogen. *Earth and Planetary Science Letters* 173, 157–170.
- Flowers, R., Ketcham, R., Shuster, D., Farley, K., 2009. Apatite (U-Th)/He thermochronometry using a radiation damage accumulation and annealing model. *Geochimica et Cosmochimica Acta* 73, 2347–2365.
- Foeken, J., Persano, C., Stuart, F., ter Voorde, M., 2007. Role of topography in isotherm perturbation: apatite (U-Th)/He and fission track results from the Malta tunnel, Tauern Window, Austria. *Tectonics* 26, TC3006. doi:[10.1029/2006TC002049](https://doi.org/10.1029/2006TC002049).
- Forsyth, D., 1985. Subsurface loading and estimates of the flexural rigidity of continental lithosphere. *Journal of Geophysical Research* 90, 12,623–12,632.
- Galbraith, R., Laslett, G., 1997. Statistical modelling of thermal annealing of fission tracks in zircon. *Chemical Geology* 140, 123–135.
- Gallagher, K., Stephenson, J., Brown, R., Holmes, C., Fitzgerald, P., 2005. Low temperature thermochronology and modeling strategies for multiple samples 1: vertical profiles. *Earth and Planetary Science Letters* 237, 193–208.
- Galy, A., France-Lanord, C., Peucker-Ehrenbrink, B., Huyghe, P., 2010. Sr-Nd-Os evidence for a stable erosion regime in the Himalaya during the past 12 Myr. *Earth and Planetary Science Letters* 290, 474–480.
- Garver, J., Brandon, M., Roden-Tice, M., Kamp, P., 1999. Exhumation history of orogenic highlands determined by detrital fission-track thermochronology. In: Ring, U., Brandon, M., Willett, S., Lister, G. (Eds.), *Exhumation Processes: Normal Faulting, Ductile Flow and Erosion*, volume 154. Geological Society, London, pp. 283–304. London, Special Publication.
- Gautam, P., Fujiwara, Y., 2000. Magnetic polarity stratigraphy of Siwalik Group sediments of Karnali River section in western Nepal. *Geophysical Journal International* 142, 812–824.
- Gautheron, C., Tassan-Got, L., Baraband, J., Pagel, M., 2009. Effect of alpha-damage annealing on apatite (U-Th)/He thermochronology. *Chemical Geology* 266, 157–170.
- Glotzbach, C., Reinecker, J., Danisik, M., Rahn, M., Frisch, W., Spiegel, C., 2008. Neogene exhumation history of the Mont Blanc massif, western Alps. *Tectonics* 27. doi:[10.1029/2007TC002247](https://doi.org/10.1029/2007TC002247).
- Glotzbach, C., van der Beek, P., Spiegel, C., 2011. Episodic exhumation of the Mont Blanc massif, Western Alps: constraints from numerical modelling of thermochronology data. *Earth and Planetary Science Letters* 304, 417–430.
- Green, P., Duddy, I., Laslett, G., Hegarty, K., Gleadow, A., Lovering, J.F., 1989. Thermal annealing of fission tracks in apatite 4. Quantitative modelling techniques and extension to geological timescales. *Chemical Geology* 79, 155–182.
- Grove, M., Harrison, T., 1996. ^{40}Ar diffusion in Fe-rich biotite. *American Mineralogist* 81, 940–951.
- Gunnell, Y., 2000. Apatite fission track thermochronology: an overview of its potential and limitations in geomorphology. *Basin Research* 12, 115–132.
- Haeuselmann, P., Granger, D., Jeannin, P.-Y., Lauritzen, S.-E., 2007. Abrupt glacial valley incision at 0.8 Ma dated from cave deposits in Switzerland. *Geology* 35, 143–146.
- Hallett, B., 1979. A theoretical model of glacial abrasion. *Journal of Glaciology* 29, 39–50.
- Hallett, B., 1996. Glacial quarrying: a simple theoretical model. *Annals of Glaciology* 22, 1–8.
- Hames, W., Bowring, S., 1994. An empirical evaluation of the argon diffusion geometry in muscovite. *Earth and Planetary Science Letters* 124, 161–169.
- Harrison, T., 1981. Diffusion of ^{40}Ar in hornblende. *Contributions to Mineralogy and Petrology* 78, 324–331.
- Herman, F., Braun, J., 2006. Fluvial response to horizontal shortening and glaciations: a study in the Southern Alps of New Zealand. *Journal of Geophysical Research* 111, F01008. doi:[10.1029/2004JF000248](https://doi.org/10.1029/2004JF000248).
- Herman, F., Braun, J., 2008. Evolution of the glacial landscape of the Southern Alps of New Zealand: insights from a glacial erosion model. *Journal of Geophysical Research* 113, F02009. doi:[10.1029/2007JF000807](https://doi.org/10.1029/2007JF000807).
- Herman, F., Braun, J., Dunlap, W., 2007. Tectono-morphic scenarios in the Southern Alps of New Zealand. *Journal of Geophysical Research* 112, B04201. doi:[10.1029/2004JB00303](https://doi.org/10.1029/2004JB00303).
- Herman, F., Cox, S., Kamp, P., 2009. Low-temperature thermochronology and thermo-kinematic modeling of deformation, exhumation, and development of topography in the central Southern Alps, New Zealand. *Tectonics* 28, TC5011. doi:[10.1029/2008TC002367](https://doi.org/10.1029/2008TC002367).
- Herman, F., Copeland, P., Avouac, J.-P., Bollinger, L., Mahéo, G., Le Fort, P., Rai, S., Foster, D., Pécher, A., Stüwe, K., Henry, P., 2010a. Exhumation, crustal deformation, and thermal structure of the Nepal Himalaya derived from the inversion of thermochronological and thermobarometric data and modeling of the topography. *Journal of Geophysical Research* 115. doi:[10.1029/2008JB006126](https://doi.org/10.1029/2008JB006126).
- Herman, F., Rhodes, E., Braun, J., 2010b. Uniform erosion rates and relief amplitude during glacial cycles in the Southern Alps of New Zealand, as revealed from OSL-thermochronology. *Earth and Planetary Science Letters* 297, 183–189.
- Hinderer, M., 2001. Late Quaternary denudation of the Alps, valley and lake fillings and modern river loads. *Geodynamics Acta* 14, 231–263.
- Hodges, K., Wobus, C., Ruhl, K., Schildgen, T., Whipple, K., 2004. Quaternary deformation, river steepening, and heavy precipitation at the front of the Higher Himalayan ranges. *Earth and Planetary Science Letters* 220, 379–389.
- House, M., Wernicke, B., Farley, K., 1998. Dating topography of the Sierra Nevada, California, using apatite (U-Th)/He ages. *Nature* 396, 66–69.
- Husson, L., Moretti, I., 2002. Thermal regime of fold and thrust belts. An application to the Bolivian Sub Andean Zone. *Tectonophysics* 345, 253–280.
- Jeffreys, H., 1931. The thermal effects of blanketing by sediments. *Geophysical Journal International* 2 (s7), 301–383.
- Ketcham, R., Donelick, R., Carlson, W., 1999. Variability of apatite fission-track annealing kinetics: III. Extrapolation to geological time scales. *American Mineralogist* 84, 1235–1255.
- Ketcham, R., Carter, A., Donelick, R., Barbarand, J., Hurford, A., 2007. Improved modeling of fission-track annealing in apatite. *American Mineralogist* 92 (5–6), 799–810.
- Kirkbride, M., Matthews, D., 1997. The role of fluvial and glacial erosion in landscape evolution: Ben Ohau range, New Zealand. *Earth Surface Processes and Landforms* 22, 317–327.
- Kohn, B., Gleadow, A., Cox, S., 1999. Denudation history of the Snowy Mountains: constraints from apatite fission track thermochronology. *Australian Journal of Earth Sciences* 46, 181–198.
- Laslett, G.M., Green, P., Duddy, I., Gleadow, A., 1987. Thermal annealing of fission tracks in apatite 2. A quantitative analysis. *Chemical Geology* 65, 1–13.
- Lawson, C., 1977. Software for c^1 surface interpolation. In: Rice, J. (Ed.), *Mathematical Software*. Academic Press, New York.
- Lock, J., Willett, S., 2008. Low-temperature thermochronologic ages in fold-and-thrust belts. *Tectonophysics* 456, 147–162.
- Lovera, O., Richter, F., Harrison, T., 1991. Diffusion domains determined by ^{39}Ar released during step heating. *Journal of Geophysical Research* 96, 2057–2069.
- Mancktelow, N., Grasemann, B., 1997. Time-dependent effects of heat advection and topography on cooling histories during erosion. *Earth and Planetary Science Letters* 147, 167–195.
- Molnar, P., England, P., 1990. Temperatures, heat flux, and frictional stress near major thrust faults. *Journal of Geophysical Research* 95, 4833–4856.
- Mugnier, J.-L., Huyghe, P., Leturmy, P., Jouanne, F., 2004. Episodicity and rates of thrust-sheet motion in the Himalayas (western Nepal). In: McClay, K.R. (Ed.), *Thrust Tectonics and Hydrocarbon Systems*, 82. AAPG Memoir, pp. 91–114.
- Mountini, G., Carcano, C., Garzanti, E., Ghielmi, M., Piccin, A., Pini, R., Rogledi, S., Sciuinnach, D., 2003. Onset of major Pleistocene glaciations in the Alps. *Geology* 31, 989–992.
- Nabelek, J., Hetenyi, G., Vergne, J., Sapkota, S., Kafle, B., Jiang, M., Su, H., Chen, J., Huang, B.-S., the Hi-CLIMB team, 2009. Underplating in the Himalaya–Tibet collision zone revealed by the Hi-CLIMB experiment. *Science* 325, 1371–1374.
- Naylor, S., Gabet, E., 2007. Valley asymmetry and glacial versus nonglacial erosion in the Bitterroot Range, Montana, USA. *Geology* 35, 375–378.
- Norris, R., Koon, P., Cooper, A., 1990. The obliquely convergent plate boundary in the South Island of New Zealand. *Journal of Structural Geology* 12, 715–725.
- Nunn, J., Aires, J., 1988. Gravity anomalies and flexure of the lithosphere at the Middle Amazon Basin, Brazil. *Journal of Geophysical Research* 93, 415–428.
- Ojha, T.P., Butler, R.F., DeCelles, P.G., Quade, J., 2009. Magnetic polarity stratigraphy of the Neogene foreland basin deposits of Nepal. *Basin Research* 21 (1), 61–90.
- Pandey, M., Tandukar, R., Avouac, J.-P., Vergne, J., Heritier, T., 1999. Seismotectonics of the Nepal Himalaya from a local seismic network. *Journal of Asian Earth Sciences* 17, 703–712.
- Pearson, O., DeCelles, P., 2005. Structural geology and regional tectonic significance of the Ramgarh thrust, Himalayan fold-thrust belt of Nepal. *Tectonics* 24, TC4008. doi:[10.1029/2003TC001617](https://doi.org/10.1029/2003TC001617).
- Rahal, J., Ehlers, T., van der Pluijm, B., 2007. Quantifying transient erosion of orogens with detrital thermochronology from syntectonic basin deposits. *Earth and Planetary Science Letters* 256 (1–2), 147–161.
- Rahn, M., Brandon, M., Batt, G., Garver, J., 2004. A zero-damage model for fission track annealing in zircon. *American Mineralogist* 89, 473–484.
- Reiners, P., Spell, T., Nicolsky, S., Zanetti, K., 2004. Zircon (U-Th)/He thermochronometry: He diffusion and comparisons with $^{40}\text{Ar}/^{39}\text{Ar}$ dating. *Geochimica et Cosmochimica Acta* 68, 1857–1887.
- Robert, X., Van der Beek, P., Braun, J., Perry, C., Dubile, M., Mugnier, J.-L., 2009. Assessing Quaternary reactivation of the Main Central Thrust Zone (Central Nepal Himalaya): new thermochronologic data and numerical modelling. *Geology* 37, 731–734.
- Robert, X., Van der Beek, P., Braun, J., Perry, C., Mugnier, J.-L., 2011. Control of detachment geometry on lateral variations in exhumation rates in the Himalaya: insights from low-temperature thermochronology and numerical modeling. *Journal of Geophysical Research* 116, B05202, 22pp. doi:[10.1029/2010JB007893](https://doi.org/10.1029/2010JB007893).
- Ruhl, K.W., Hodges, K.V., 2005. The use of detrital mineral cooling ages to evaluate steady state assumptions in active orogens: an example from the central Nepalese Himalaya. *Tectonics* 24. doi:[10.1029/2004TC001712](https://doi.org/10.1029/2004TC001712).
- Sambridge, M., 1999a. Geophysical inversion with a Neighbourhood Algorithm – I. Searching a parameter space. *Geophysical Journal International* 138, 479–494.
- Sambridge, M., 1999b. Geophysical inversion with a Neighbourhood Algorithm – II. Appraising the ensemble. *Geophysical Journal International* 138, 727–746.
- Schildgen, T., Ehlers, T., Whipple, K., van Soest, M., Whipple, K., Hodges, K., 2009. Quantifying canyon incision and Andean Plateau surface uplift, southwest Peru: a

- thermochronometer and numerical modeling approach. *Journal of Geophysical Research* 114, F04014. doi:[10.1029/2009F001305](https://doi.org/10.1029/2009F001305).
- Schildgen, T.F., Balco, G., Shuster, D.L., 2010. Canyon incision and knickpoint propagation recorded by apatite $^{40}\text{He}/^{3}\text{He}$ thermochronometry. *Earth and Planetary Science Letters* 293 (3–4), 377–387.
- Schwarz, G., 1978. Estimating the dimension of a model. *The Annals of Statistics* 6, 461–464.
- Shi, Y., Allis, R., Davey, F., 1996. Thermal modelling of the Southern Alps, New Zealand. *Pure and Applied Geophysics* 146, 469–501.
- Shuster, D., Farley, K., 2004. $^{40}\text{He}/^{3}\text{He}$ thermochronometry. *Earth and Planetary Science Letters* 217, 1–17.
- Shuster, D.L., Cuffey, K.M., Sanders, J.W., Balco, G., 2011. Thermochronometry reveals headward propagation of erosion in an alpine landscape. *Science* 332 (6025), 84–88.
- Simon-Labric, T. (2010). Evolution du refroidissement, de l'exhumation et de la topographie des arcs magmatiques actifs: approches par thermochronologie et modélisation numérique. Exemple des North Cascades (U.S.A.) et de la zone de faille Motagua (Guatemala). Unpublished PhD thesis, Université de Lausanne, Lausanne, Switzerland.
- Smith, E., Stern, T., O'Brien, B., 1995. A seismic velocity profile across the central South Island, New Zealand, from explosion data. *New Zealand Journal of Geology and Geophysics* 38, 565–570.
- Stephenson, J., Gallagher, K., Holmes, C., 2006. A Bayesian approach to calibrating apatite fission track annealing models for laboratory and geological timescales. *Geochimica et Cosmochimica Acta* 70, 5183–5200.
- Stüwe, K., White, L., Brown, R., 1994. The influence of eroding topography on steady-state isotherms. Application to fission track analysis. *Earth and Planetary Science Letters* 124, 63–74.
- Suggate, R.P., Almond, P.C., 2005. The Last Glacial Maximum (LGM) in western South Island, New Zealand: implications for the global LGM and MIS 2. *Quaternary Science Reviews* 24 (16–17), 1923–1940.
- Szulc, A.G., Najman, Y., Sinclair, H., Pringle, M., Bickle, M., Chapman, H., Garzanti, E., Ando, S., Huyghe, P., Mugnier, J.L., Ojha, T.P., DeCelles, P.G., 2006. Tectonic evolution of the Himalaya constrained by detrital $^{40}\text{Ar}/^{39}\text{Ar}$, Sm–Nd and petrographic data from the Siwalik foreland basin succession, SW Nepal. *Basin Research* 18, 375–391.
- Tagami, T., Galbraith, R., Yamada, R., Laslett, G., 1998. Revised annealing kinetics of fission tracks in zircon and geological implications. In: Van den Haute, P., De Corte, F. (Eds.), *Advances in Fission-Track Geochronology*. Kluwer Academic Publishers, Dordrecht, the Netherlands, pp. 99–112.
- Tarantola, A., 2005. *Inverse Problem Theory and Model Parameter Estimation*. Society for Industrial and Applied Mathematics, Philadelphia.
- Toy, V.G., Craw, D., Cooper, A.F., Norris, R.J., 2010. Thermal regime in the central Alpine Fault zone, New Zealand: constraints from microstructures, biotite chemistry and fluid inclusion data. *Tectonophysics* 485 (1–4), 178–192.
- Tranel, L.M., Spotila, J.A., Kowalewski, M.J., Waller, C.M., 2011. Spatial variation of erosion in a small, glaciated basin in the Teton Range, Wyoming, based on detrital apatite (U–Th)/He thermochronology. *Basin Res.* 23, 571–590. doi:[10.1111/j.1365-2117.2011.00502.x](https://doi.org/10.1111/j.1365-2117.2011.00502.x).
- Valla, P., Herman, F., Van der Beek, P., Braun, J., 2010. Inversion of thermochronological age-elevation profiles to extract independent estimates of denudation and relief history – I: theory and conceptual model. *Earth and Planetary Science Letters* 295, 511–522.
- Valla, P.G., van der Beek, P.A., Braun, J., 2011. Rethinking low-temperature thermochronology data sampling strategies for quantification of denudation and relief histories: a case study in the French western Alps. *Earth Planet. Sci. Lett.* 307, 309–322. doi:[10.1016/j.epsl.2011.05.003](https://doi.org/10.1016/j.epsl.2011.05.003).
- Valla, P.G., van der Beek, P.A., Shuster, D.L., Braun, J., Herman, F., Tassan-Got, L., Gautheron, C., 2012. Late Neogene exhumation and relief development of the Aar and Aiguilles Rouges massifs (Swiss Alps) from low-temperature thermochronology modeling and $^{40}\text{He}/^{3}\text{He}$ thermochronometry. *J. Geophys. Res.* 116. doi:[10.1029/2011F002043](https://doi.org/10.1029/2011F002043).
- van der Beek, P., Bourbon, P., 2008. A quantification of the glacial imprint on relief development in the French western Alps. *Geomorphology* 97, 52–72.
- van der Beek, P., Braun, J., 1998. Numerical modelling of landscape evolution on geological time scales: a parameter analysis and comparison with the southeastern highlands of Australia. *Basin Research* 10, 49–68.
- van der Beek, P., Valla, P., Herman, F., Braun, J., Persano, C., Dobson, K., Labrin, E., 2010. Inversion of thermochronological age-elevation profiles to extract independent estimates of denudation and relief history – II: application to the French Western Alps. *Earth and Planetary Science Letters* 296, 9–22.
- Vermeesch, P., 2007. Quantitative geomorphology of the White Mountains (California) using detrital apatite fission track thermochronology. *Journal of Geophysical Research* 112 (F03004). doi:[10.1029/2006F000671](https://doi.org/10.1029/2006F000671).
- Vetterling, W.T., Press, W.H., Teukolsky, S.A., Flannery, B.P., 1992. *Numerical Recipes*, 2nd Ed. Cambridge University Press, New York, volume.
- Wagner, G., Reimer, G., 1972. Fission-track tectonics: the tectonic interpretation of fission track ages. *Earth and Planetary Science Letters* 14, 263–268.
- Whipp, D., Ehlers, T., 2007. Influence of groundwater flow on thermochronometer-derived exhumation rates in the central Nepalese Himalaya. *Geology* 35, 851–854.
- Whipp, D., Ehlers, T.A., Blythe, A.E., Huntington, K.W., Hodges, K.V., Burbank, D.W., 2007. Plio–Quaternary exhumation history of the central Nepalese Himalaya: 2. Thermokinematic and thermochronometer age prediction model. *Tectonics* 26 (TC3003).
- Whipp, D., Ehlers, T., Braun, J., Spath, C., 2009. Effects of exhumation kinematics and topographic evolution on detrital thermochronometer data. *Journal of Geophysical Research* 114, F04021. doi:[10.1029/1008F001195](https://doi.org/10.1029/1008F001195).
- Whipple, K., 2009. The influence of climate on the tectonic evolution of mountain belts. *Nature Geoscience* 2, 97–104.
- Whipple, K., Kirby, E., Brocklehurst, S., 1999. Geomorphic limits to climate-induced increases in topographic relief. *Nature* 401, 39–43.
- Wobus, C.W., Hodges, K.V., Whipple, K.X., 2003. Has focused denudation sustained active thrusting at the Himalayan topographic front? *Geology* 31, 861–864.
- Wobus, C.W., Whipple, K., Hodges, K.V., 2006. Neotectonics of the central Nepalese Himalaya: constraints from geomorphology, detrital $^{40}\text{Ar}/^{39}\text{Ar}$ thermochronology, and thermal modeling. *Tectonics* 25. doi:[10.1029/2005TC001935](https://doi.org/10.1029/2005TC001935).
- Wolf, R., Farley, K., Kass, D.M., 1998. Modeling of the temperature sensitivity of the apatite (U–Th)/He thermochronometer. *Computational Geosciences* 148, 105–114.